

Modelling of gyro in an IR seeker for real-time simulation

Examensarbete utfört i Reglerteknik
vid Tekniska Högskolan i Linköping
av

Thomas Nordman

Reg nr: LiTH-ISY-EX-3426
Linköping 2004

Modelling of gyro in an IR seeker for real-time simulation

Examensarbete utfört i Reglerteknik
vid Tekniska Högskolan i Linköping
av

Thomas Nordman

Reg nr: LiTH-ISY-EX-3426

Supervisor: **Lars Tydén**
Johan Sjöberg

Examiner: **Anders Helmersson**

Linköping 19th January 2004.

Abstract

The target tracking system of an IR (InfraRed) guided missile is constantly subjected to disturbances due to the linear and angular motion of the missile. To diminish these LOS (Line Of Sight) disturbances the seeker of the missile can be built from a free gyroscope mounted in a very low friction suspension. The ability of the spinning gyroscope to maintain its direction relative to an inertial frame is used to stabilize the seeker LOS while tracking a target.

The tracking velocity of the seeker, i.e. its angular velocity, is controlled by a feedback control unit where the signal from the IR detector is used as input. The electrical driven actuator consists of a set of coils and a magnet on the gyroscope.

The purpose of this thesis is to develop a real-time model of the seeker gyroscope in an existing IR MANPAD (MAN Portable Air Defense) missile. The aim is a model that is able to simulate the real system with consideration to the tracking velocity. The model should also be integrated into a hybrid simulator environment.

With relatively good knowledge of the system and its subsystems an initial physical modelling approach was used where elementary equations and accepted relations were assembled to describe the mechanism of the subsystems. This formed the framework of the model and gave a good foundation for further modelling. By using experimentation and more detailed system knowledge the initial approach could be developed and modified. Necessary approximations were made and unknown parameters were determined through system identification methods. The model was implemented in MATLAB[®] Simulink[®]. To make it suitable for real-time operation Real-Time Workshop[®] was used.

The model design was evaluated in simulations where the tracking performance could be tested for different positions of the gyroscope. The results were satisfying and showed that the model was able to reproduce the output of the system well considering the speed of the model and the approximations made. One important reason that good results can be achieved with a relatively simple model is that the seeker is limited to small rotations. The model can be tuned to operate in a smaller range and the complexity can be kept low. A weakness of the model is that the output error increases for wide angles.

Keywords: gyroscope, real-time model, modelling, seeker, HWIL, IR missile

Sammanfattning

Målföljarsystemet hos en IR (InfraRöd)-styrd robot är ständigt föremål för störningar på grund av linjär- och rotationsrörelse hos roboten. För att minska dessa siktlinjestörningar kan robotens målsökare byggas av ett fritt gyro monterad i en upphängning med mycket låg friktion. Förmågan hos det spinnande gyrot att behålla sin riktning relativt ett absolut koordinatsystem används för att stabilisera målsökarens siktlinje under målföljning.

Målsökarens följehastigheten, d.v.s. vinkelhastigheten, styrs av ett återkopplat regelsystem där signalen från IR-detektorn används som insignal. Den elektriskt drivna aktuatoren består av en uppsättning spolar och en magnet på gyrot.

Syftet med den här rapporten är att utveckla en realtidsmodell av målsökargyrot i en befintlig IR MANPAD (eng. MAN Portable Air Defense) robot. Målet är en modell som simulerar det verkliga systemet med avseende på följehastigheten. Modellen ska även integreras i en hybridsimulatormiljö.

Med realitvt god kunskap om systemet och dess delsystem gjordes en inledande fysikalisk modelleringsansats där elementära ekvationer och vedertagna relationer användes för att beskriva mekanismen hos delsystemen. Detta utgjorde modellens ramverk och skapade en bra grund för fortsatt modellering. Genom experimentering och mer detaljerad kunskap om systemet kunde den inledande ansatsen utvecklas och modifieras. Nödvändiga approximationer infördes och okända parametrar bestämdes genom systemidentifieringsmetoder. Modellen implementerades i MATLAB[®] Simulink[®]. För att anpassa den till körning i realtid användes Real-Time Workshop[®].

Modeldesignen utvärderades i simuleringar där målföljningsprestanda kunde testas för olika positioner hos gyrot. Resultaten var tillfredsställande och visade att modellen kunde reproducera systemets utsignal väl med hänsyn till modellens snabbhet och de approximationer som gjorts. En viktig anledning till att goda resultat kan nås med en relativt enkel modell är att målsökaren har en begränsad utvridning. Modellen kan anpassas till ett mindre arbetsområde och komplexiteten kan hållas nere. En svaghet hos modellen är att felet i utsignalen ökar för större vinklar.

Acknowledgements

I would like to thank my supervisor at FOI, Lars Tydén for giving me the opportunity to take part in his project working with this master thesis, and for the guidance and support that made it possible. Also I would like to thank my supervisor at LiTH, Johan Sjöberg for his commitment and good advises that helped me through the work. Thank you both for your patience.

Great thanks to my co-worker in the HWIL project, Mathias Bergvall, for valuable discussions and his help concerning the hybrid simulator interface. Per Holm, my opponent, deserves gratitude for his good remarks.

The months at FOI with the people at department of Electronic Warfare Assessment has been enjoyable. Thank you all for the inspiration and friendly atmosphere during this time.

Finally I would like to thank my family and people close to me (you know who you are) for their love and support throughout the years.

Notation

Important Symbols

\mathbf{x}, \mathbf{X}	Boldface letters are used for vectors and matrices.
\mathbf{x}^T	Transpose.
\mathbf{C}_{AB}	Rotation of the A-frame relative the B-frame using yaw and pitch.
\mathbf{d}_{xAB}	Rotation of the A-frame x-axis relative to the B-frame using spherical angles.
θ_p, ϕ_y	Pitch, yaw.
θ_{sph}, ϕ_{sph}	Spherical angles.
$\mathbf{\Omega}$	Precession velocity of gyroscope.
\mathbf{M}	Applied torque.
\mathbf{m}	Magnetic dipole moment.
\mathbf{B}	Magnetic field.
ω_{ref}	Spin-rate of gyroscope along the seeker x-axis.
p_x	Approximated spin-rate along the seeker x-axis (constant).
I	Moment of inertia of the seeker along its x-axis.

Abbreviations

AC	Alternating Current.
A/D	Analog to Digital.
API	Application Program Interface.
D/A	Digital to Analog.
I/O	Input-Output.
FOV	Field Of View.
GUI	Graphical User Interface.
IR	InfraRed.
LOS	Line Of Sight.
HWIL	HardWare In the Loop.
MANPAD	MAN Portable Air Defense.
RTW	Real-Time Workshop®.

Contents

1	Introduction	1
1.1	Background	1
1.2	Objectives	1
1.3	Method	2
2	The Hybrid Simulator	3
2.1	The MANPAD Weapon System	3
2.1.1	The Launch System	3
2.1.2	The Missile	4
2.1.3	The IR Seeker	5
2.2	Simulator Overview	5
2.2.1	Buffered Signal Processing	7
2.2.2	Instrumentation	8
2.3	The Operating System	8
3	System Description	11
3.1	Problem Description	11
3.2	The Seeker Control Loop	12
3.3	The Gyroscope	12
3.3.1	The Permanent Magnet	13
3.4	The Coils	14
4	The Model Framework	17
4.1	Model Building Aspects	17
4.2	Modelling Outline	17
4.3	Representation	19
4.3.1	Reference Frames	19
4.3.2	Euler Angles	20
4.4	System Dynamics	24
4.4.1	Equations of Motion	24
4.4.2	Steady Precession	26
4.5	Electromagnetics	27
4.5.1	Magnetic Dipole Moment	27

4.5.2	Magnetic Fields	28
4.5.3	Magnetic Torque	29
5	Model Construction	31
5.1	Dynamics	31
5.1.1	Steady State Approximation	31
5.2	The State Space Description	34
5.2.1	Position Update Approximation	36
5.3	Modelling the Coils	37
5.3.1	The Spin Coils	37
5.3.2	The Precession Coils	42
5.4	Parameter Estimation	45
6	Implementation and Validation	49
6.1	Implementation	49
6.1.1	Simulink®	49
6.1.2	Real-Time Workshop®	56
6.2	Validation	59
6.2.1	Step-Response and Target Tracking	59
6.2.2	Comments on the Plots	60
7	Conclusions	67
7.1	Future Work	68
	Bibliography	70
A	Supplementary Subsystems of the Model	71
B	Functions Generated by Real-Time Workshop®	73

Chapter 1

Introduction

1.1 Background

Advanced high performing simulators are considered as standard tools in many areas of research and development. Simulations are used for various purposes, and different simulators also have different requirements. In many cases the run time of a simulation is crucial. This is especially true for simulators in real-time systems. A real-time simulator is useful (and necessary) in several different applications and as the computational capacity and overall performance of computers steadily improves, they become more and more sophisticated.

Areas of research within FOI (The Swedish Defence Research Agency) include the analysis and evaluation of systems and system technique with consideration to electronic warfare. In electronic warfare different means of signal intelligence and electronic counter measures are used to gain advantage on the battlefield. Modelling and simulation plays an important role in the assessment of the often very complex electronic warfare duels. As part of the research, a project developing the methodology for hybrid simulations with IR (InfraRed) MANPAD (MAN Portable Air Defense) missiles is currently progressing. This simulator is built as a HWIL (HardWare In the Loop) simulator, where the seeker electronics from the missile are kept as external units, while seeker dynamics, sensors and other functions are modelled. One aim with the project is to gain knowledge about the performance of the missile seeker, another is to develop countermeasures and perform tests. A simulator of this kind will also be beneficial when validating already implemented models with consideration to the methods used.

1.2 Objectives

The objective of this master thesis is to develop and validate a real-time model of the seeker gyroscope in the MANPAD missile. The model should also be incorporated into the simulator environment. Furthermore, this work aims to develop and

describe a method for constructing a model of the seeker gyroscope from the given lab bench. The method can then be used for modelling future systems.

1.3 Method

The preliminary research mainly involved studying related work and literature on mechanics and electromagnetic theory. Developing a method also meant that effort was put into examining possible modelling tools and ways to implement the model. Among the factors that had to be considered were run-time environment and requirements, and model modularity, but also the chosen modelling procedure.

Chapter 2

The Hybrid Simulator

This chapter serves as a more complete introduction to the parts of the project that are relevant to this thesis. The components of the simulator are described in short as well as some basic technical solutions. The latter includes instrumentation and signal processing. More detailed information is found in [14].

2.1 The MANPAD Weapon System

To build the HWIL simulator, a MANPAD weapon system is modified and prepared for instrumentation and measurement. MANPAD is short-term for Man-portable air defense and is a weapon system that enables a gunner on ground to launch infrared guided missiles, IR missiles. The system consists of an IR missile and a launch tube with a gripstock.

2.1.1 The Launch System

The launch tube assembly is a fibreglass tube which houses the missile. It provides the means to transport, aim and fire the missile. The launch tube provides the main support for all other parts of the weapon system. Both ends of the tube are sealed with breakable disks to protect the missile from dust and damp. The front disk is transparent to IR radiation, allowing the radiation to reach the heat-sensitive missile seeker. The disks break at launch. At the front end of the tube there are current-carrying coils that are used to give the seeker gyroscope its rotational speed prior to launch of the missile. These are further explained in Section 3.4. A hinged sight with a protective eye shield is attached to the tube and allows the gunner to sight the weapon, determine target range and superelevate the weapon. The sight assembly also consists of an indicator through which audible tones can be heard. The tone changes depending on the direction of the seeker relative to the IR source. While sighting the weapon the seeker is locked in the center of the missile pointing straight ahead. Before launching the missile the seeker can be released (uncaged) through a switch and the indicator allows the gunner to determine if the seeker is

tracking the target. The electrical system needed for activating and launching the missile are contained inside the gripstock. Located on the gripstock assembly are the controls; safety and actuator device, the uncaging switch and the firing trigger. Connected to the actuator is a replaceable battery coolant cartridge. Loaded into the gripstock, it supplies power to the electrical circuits and is used to cool the IR detector in the seeker prior to the launch of the missile. The cartridge consists of a battery and a pressurized gas coolant.

2.1.2 The Missile

The missile is divided into three sections; the guidance section, the warhead section and the propulsion section.

The propulsion of the missile is provided by a launch motor and a thrust flight motor. During the first stage, the launch motor gives an initial thrust to the missile that ejects it from the launch tube. This allows the missile to travel a safe distance from the gunner before the second stage where the flight motor is ignited. The ignition is controlled by timers and accelerometers. The flight motor provides thrust to accelerate the missile to its cruise speed.

The warhead section consists of a fuse assembly and explosives. While still inside the launch tube and during launch, the warhead is secured. To arm it, both launch and flight motor must have been ignited giving the missile its expected acceleration. Should the missile not intercept a target within a specific time range after launch, a self-destruct circuit automatically initiates warhead detonation.

The guidance and control system is located in the front part of the missile and consists of the seeker, the guidance control unit and the rudders. The seeker receives IR radiation emitted from a heat source, typically the engine of an air target, and converts this energy into an electric signal. The signal processed in the guidance control unit which calculates control signals to the gyroscope of the seeker and the rudders. The rudders and the tail fins are in a folded position in the launch tube, and as the missile is launched they are erected and locked into place. The

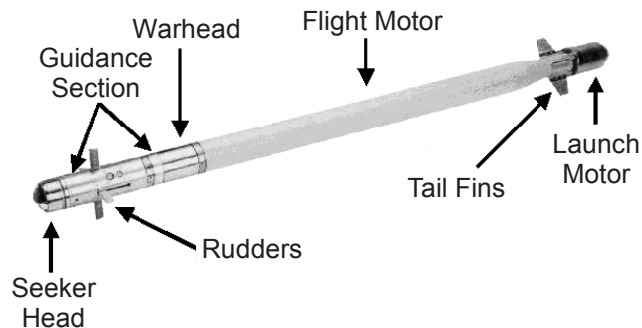


Figure 2.1: The IR missile.

tail fins provide a roll to stabilize the missile and to steer it in a certain direction two of the rudders changes direction at the same rate as this rolling rotation.

The guidance section is the central part of the simulator and is left intact, while modifications include the removal of both the warhead section and propulsion section. The seeker and the guidance control unit are more thoroughly explained in the next section. A typical IR missile is depicted in Figure 2.1.

2.1.3 The IR Seeker

The seeker is placed behind a glass dome that is located in the front end of the body of the missile. Incoming radiation is focused by gimballed optics (i.e. supported on gimbals) consisting of a primary and secondary mirror located on a gyroscope. The concentrated beam is then modulated by a reticle before it is collected on the IR sensitive detector. The reticle is a small circular disk that contains a spatial pattern of transmitting and non-transmitting fields. The detector signal is modulated with information indicating target position relative to the seeker LOS (Line Of Sight). So called nutation scanning is used, in which the image of a point source is moved around a circle of fixed radius R at the nutation frequency f over the fixed reticle. The center of the nutation circle corresponds to the target position in the field of view. It follows that the circle of a target along the LOS is concentric, see Figure 2.2. This motion is due to an offset in the rotating optics, and the nutation frequency equals the spin-rate of the gyroscope. The target image generates pulses as it moves over the reticle pattern and as the pulse-width varies over the nutation cycle a recoverable frequency and amplitude modulation is produced. The detector produces an electrical signal proportional to the amount of incident radiant power. The seeker electronics amplify the detector signal and demodulate it to recover an error signal. Control signals are then calculated and fed to the gyroscope and the control surfaces (rudders). The seeker is kept looking at (or tracking) the target, while the missile is steered with the rudders. The signal processing in the missile is illustrated in Figure 2.2.

A comprehensive description of IR seekers and IR tracking systems in general is found in [15].

2.2 Simulator Overview

While developing the model a first version of the simulator was used. The simulator included the real gyroscope to enable simulations without a gyro model. In this way data could be obtained from the system to gain knowledge and to validate the model. Since target radiation, seeker optics and reticle are modelled and described by the simulated detector signal, the purpose of the real gyro system is solely to provide position information.

Here follows a brief description of the signal processing in the HWIL system. Only parts relevant to the gyro model are considered. The block structure of the implementation is shown in Figure 2.3.

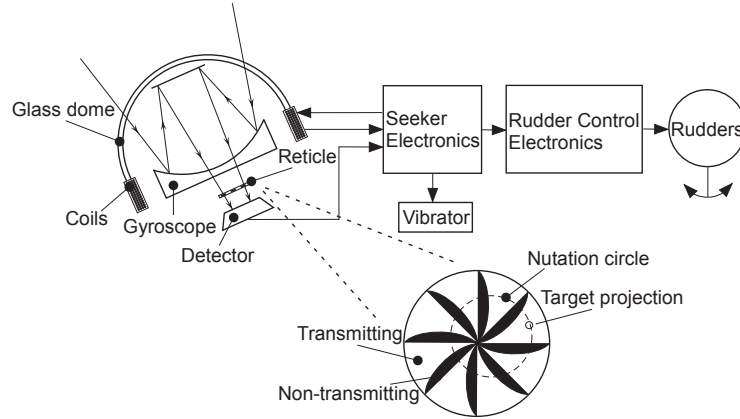


Figure 2.2: Signal processing and reticle in the missile.

Estimator

The estimator block processes samples read from the A/D converter. The sampled signals include the cage signal **cage** (gyroscope position), reference signal **ref** (gyroscope rotation relative to the missile), the currents in the precession coils \mathbf{l}_1 , \mathbf{l}_2 and the IR detector signal **d**. The following is estimated from the samples

- Frequency of the reference signal, $\mathbf{ref}_{\text{freq}}$
- Starting time, i.e. phase, of the detector signal relative to the reference signal, $\mathbf{d}_{\text{phase}}$
- Amplitude and phase of the cage signal, $\mathbf{cage}_{\text{ampl}}$, $\mathbf{cage}_{\text{phase}}$
- Roll angle of the gyroscope, **roll**

The phase of the cage signal is estimated with sub-sample resolution by interpolating between sample points in the zero transition. This is necessary to get an adequate accuracy of the position of the gyroscope.

Sync

The output is synchronized with the reference signal by adjusting the length (period) of the precalculated signal, i.e. the number of samples written to the D/A output buffer. The length is controlled by a PI-regulator that calculates the extent of the adjustment.

GyroPos

GyroPos uses the phase and amplitude of the cage signal to calculate the position of the gyroscope.

GyroModel

The model receives the measured currents from the precession coils (i.e. the control signals) along with the estimated roll angle of the gyroscope.

Target

Target position is given in absolute coordinates and is calculated from angles specified relative to the seeker. The distance between target and seeker is set to a fixed value.

Synthesis

Synthesis calculates the IR detector signal that is put in the D/A output buffer and later used by the seeker electronics. Instead of precalculating the signal for a complete revolution, the length of the generated signal only corresponds to about 20% of a revolution. It is thus updated more often and a quicker response to changes in gyro position is gained. The signal is generated by modelling the function of the reticle. Outputs from GyroPos or the GyroModel and Target are used to calculate a nutation circle over a reticle image. Samples are then read from the circle in the same manner as the real signal is sampled. The output from Sync determines the length of the signal in number of samples. The buffered signal processing in the HWIL simulator is further described in Section 2.2.1.

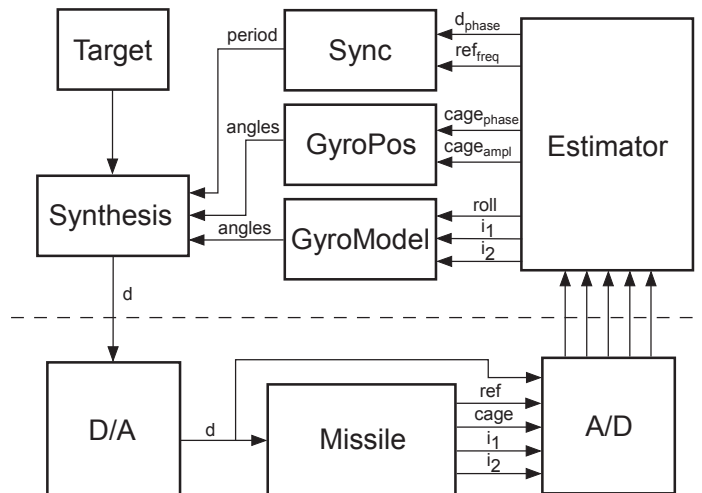


Figure 2.3: Simulator overview. Blocks above the dashed line are implemented in software while blocks below the line are implemented in hardware.

2.2.1 Buffered Signal Processing

The HWIL simulator utilizes buffered data acquisition and signal generation. This means that a series of data samples is read from the A/D converter or written to the D/A converter during each data transfer. Buffering enables higher sampling

rates by reducing the processor time used for communication with the I/O card. With the given configuration and a sampling rate of 40 kHz, only a fraction of the processor capacity is used for data transfer and thus allowing sufficient processor time for model simulation and signal processing. Since a signal from the seeker is sampled at 40 kHz and the gyroscope is assumed to have a constant rotation velocity of 100 revolutions per second, one revolution corresponds to 400 samples. Buffers of 40 samples are read from the A/D converter at rate of 1 kHz, i.e. 10 times during one revolution. Normally the seeker electronics receives a signal from the IR detector as was described in Section 2.1.3, but during the simulation a simulated detector signal is used instead. The simulated signal is precalculated for approximately 1/5 of a revolution and thus 80 samples are written to the D/A converter each time. The calculation and update of the detector signal is done when the number of samples in the D/A output buffer falls below a specified threshold. The rotation velocity of the gyroscope varies and is not always 100 revolutions per second which results in a variation of the number of samples per revolution. The variation makes it necessary to synchronize the generated signal with a reference.

2.2.2 Instrumentation

The fundamental property of the HWIL simulator is the interaction between computer and hardware. Analog signals from the seeker are measured, processed and converted to be used in the implemented model. Signals must also be generated and fed back to the hardware. The simulator uses three synchronized I/O cards for conversion between analog and digital formats. The properties of the measured and generated signals are important and specify requirements on the A/D converters. In addition to the I/O cards a signal conditioning system is required to make the signals suitable for conversion. Signal conditioning plays a major role in producing accurate and stable measurements. A few important functions are performed. Most importantly the conditioning circuits amplify the signals to levels within the dynamic range of the I/O card to improve accuracy. Furthermore, conditioning ensures high input impedance relative to the source impedance. This is necessary to avoid that input signals are affected when measured.

2.3 The Operating System

The simulator is implemented in a PC workstation running Windows XP with Venturcom RTX. RTX is a real-time extension for Windows that improves task scheduling and timing control. The timing demand on the operating system is important. The point in time when application addresses the D/A converter, and by that means delivers a signal to the hardware, needs to be precise. The reason for this is the high rotational velocity of the gyroscope. The rotation-rate is 100 revolutions per second, meaning that a single revolution is completed in 10 milliseconds. The generated signal that is fed to the D/A buffer must be continuous over one full turn. This implies that the signal segments of 80 samples (described

in Section 2.2.1) should coincide and hence that the time delay between them must be negligible. The detector signal must also be synchronized with the gyroscope. If not, the difference in phase will be interpreted by the seeker electronics as a position displacement that in the end results in incorrect control signals. Synchronization of the generated signal was described in Section 2.2.

Interrupt latencies in Windows can be very good, averaging less than 25 microseconds. The problem is however that there is no bound on the worst-case interrupt latencies, and these can exceed 5 milliseconds. This means that when a task is requested, the time taken to the actual execution can range from a few microseconds to milliseconds. RTX, on the other hand, provides a deterministic response capability, where request calls are completed in less than 5 microseconds. Processes are executed in the RTX real-time subsystem (RTSS), which have higher priority than other Windows applications running simultaneously. If time consuming calculations must be performed in a RTSS application and a Windows application at the same time, the RTSS process is allotted 100% of the processor capacity.

Chapter 3

System Description

The system of current interest consists of a magnetic gyroscope and current carrying coils. These subsystems are described in this chapter. As a starting point the purpose of the model is presented.

3.1 Problem Description

The HWIL concept enables integration of real systems into computer-based simulations. When possible, using the actual system instead of a model of it obviously improves the performance of a simulator. The HWIL simulator used in the project integrates the seeker of an IR missile into a simulation environment. By modelling and simulating the signal from the IR sensitive detector the gyroscope can be controlled. The simulated signal is input to the guidance control system and corresponds to a target in the seeker FOV (Field Of View). The guidance system computes the control signals that direct the seeker LOS at the target. The detector signal can be calculated by using information about the position of the gyroscope and the (simulated) target (see Section 2.2).

The usefulness of the simulator is limited when the missile and the seeker is fixed to a lab bench. The aim is of course to simulate a scenario where a missile in flight interacts with targets and countermeasures. Since such a simulation involves missile dynamics the fixed gyro system can not be used. The reason is that the orientation of the gyroscope relative to the missile depends on missile orientation relative to an inertial reference system. If the missile turns, the orientation of the rotor axis of the gyroscope stays fixed relative to the inertial frame and thus changes its position relative to the missile. This is due to a fundamental property of gyroscopes. This is described in Section 3.3. The simulation of a flying IR missile can be done in one of two ways; by setting the entire missile body in motion or by modelling and implementing the gyro system as a part of a missile model in software. The former can be realized by using a industrial robot. However, this is extremely expensive and the missiles easily get worn out. The latter method is more convenient in this

case and also the one employed. The models are built and implemented in the HWIL environment to be simulated with hardware.

3.2 The Seeker Control Loop

The guidance section in the missile uses a feedback control loop to control the position of the gyroscope. This control loop consists of the seeker electronics and the gyro system.

As was described in Section 2.1.3, the modulated signal from the detector contains information about the position of the target relative the LOS of the seeker. This signal is amplified and demodulated by the seeker electronics producing an error signal. The error signal is then used to calculate the control signal that is fed to the gyro system. The purpose of the controllable gyroscope is to prevent the target from escaping outside the view of the seeker. This property is important since the seeker has a limited FOV. A schematic diagram of the seeker control loop is shown in Figure 3.1. The diagram show how the model will be used in the simulator.

The gyro system consisting of the magnetic gyroscope and the coils are treated in the sections to follow.

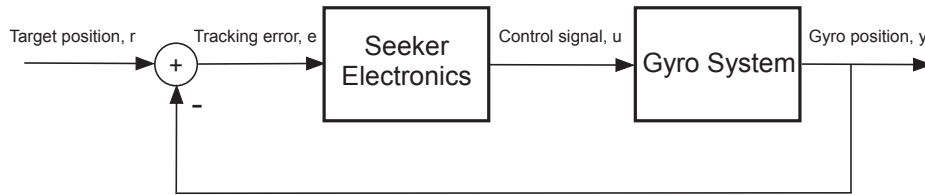


Figure 3.1: The control loop of the seeker system. The demodulation and calculation of the error signal is simplified.

3.3 The Gyroscope

Tracking systems that operate from non-stationary platforms are subjected to angular disturbances that results from linear and angular motion of the platform. These line-of-sight disturbances are direct inputs to the tracking system and are usually attenuated by some means [15]. To diminish the effects of a moving platform stabilization subsystems are generally utilized. The free gyroscope in the missile seeker constitutes such a subsystem. The capability of the free gyroscope to maintain a fixed direction is used to keep the LOS vector directed at the target. The gyroscope is mounted in a Cardan's suspension, which permits unconstrained rotation. The assembly consists of a rotor, where the mass of the gyroscope is concentrated, and outer and inner gimbals. The most common Cardan's suspension is shown in Figure 3.2. Although the principle is the same the mounting used in the seeker is different from that in the figure. The rotor spins about the axis directed

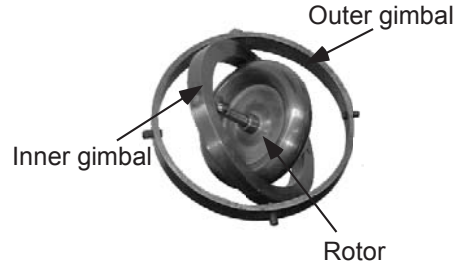


Figure 3.2: A gyroscope mounted in a Cardan's suspension.

along the LOS vector. The mass center of the gyroscope is located in the assembly center point, i.e. where the three axes of rotation intersect. Assuming that all of the bearings have negligible friction and no external moments are applied to the gimbals, the motion of the rotor is torque-free [13]. If the rotor of the gyroscope is spinning about a certain axis, the angular momentum \mathbf{H} will also be directed along this same axis. Since the motion is torque-free, the direction of the rotor axis will remain fixed according to the relation [13], [9]

$$\sum \mathbf{M} = \frac{d\mathbf{H}}{dt} = 0$$

It follows that the direction of the gyroscope is independent of missile acceleration and the earth gravitational force [2]. Besides the stabilization capabilities the gyroscope has the important function of being the pointing assembly of the seeker system. The gyroscope is free to rotate and is used to direct the detector at the target. The rotation is limited to about 15 degrees.

3.3.1 The Permanent Magnet

Torque is the driving parameter for this rotational system. The electrical driven actuator that provides this torque consists of a set of coils and a permanent magnet. The circular shaped magnet is located on the outer rim of the rotor. The magnetic property of a permanent magnet is determined by \mathbf{m} , the so called magnetic dipole moment. It can be calculated using [1]

$$\mathbf{m} = \mathbf{M}V \quad (3.1)$$

Where \mathbf{M} is a material specific parameter interpreted as the magnetic dipole moment density and V is the total volume of the magnet. In addition, the inertial properties of the gyroscope can be considered to be determined by the inertial properties of the magnet, where the mass of the rotor is concentrated. To be able to calculate \mathbf{M} , V and the moments of inertia \mathbf{I} , the geometry of the magnet is approximated by a cylindrical shell. The material is assumed to be a compound of iron (99%) and carbon, i.e. ordinary steel [12].

3.4 The Coils

A number of coils are placed around the gyroscope for actuating and measuring purposes. These are loops of conducting wire that are fixed to the missile body or the launch tube. The coils fixed to the missile is depicted in Figure 3.3. By running an electrical current through the coils, a magnetic field is created. The permanent magnet placed inside this field will experience a torque that tends to rotate it. Coils included in the missile weapon system are

- Precession coils (seeker system)
- Cage coil (seeker system)
- Reference coils (seeker system)
- Spin coils (launch tube)

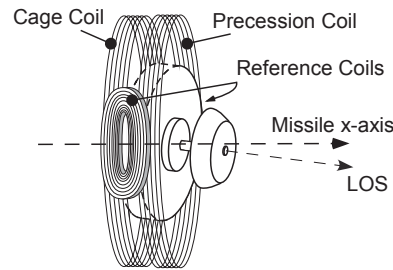


Figure 3.3: The coils in the missile.

The precession coils are fed with the control signal from the seeker electronics and are thus the primary coils when modelling the dynamics of the gyroscope. These coils provide a torque that makes the spinning gyroscope precess or turn about axes perpendicular to the spin axis. To reduce undesirable effects and to create a more uniform magnetic field, two coils with opposite windings are used. The coils carry currents that are phase-shifted 180 degrees relative to each other. The cage coil is located next to the precession coils and measures the position of the rotor of the gyroscope including the spin angle. The rotation of the magnetic rotor induces an electromagnetic force and hence a current in the coil according to Faraday's law. This periodic signal is referred to as the cage signal.

Reference coils are placed on each side of the gyroscope. These coils measure the rotation (spin) of the rotor relative to the missile (i.e. gyro spin + missile roll). The induced reference signal has a period that corresponds to one full revolution of the rotor.

Prior to the launch the gyroscope is set spinning by a pair of spin coils. These are located in the launch tube and are positioned in the same manner as the reference coils. The principle of operation is that of an electrical (AC) motor with a rotor and a stator. The time-varying magnetic field produced by the coils results in a

torque that rotates the magnetic rotor about its axis of symmetry. As the missile leaves the launch tube the spin-rate of the gyroscope slowly starts to decrease and continues to do so during flight.

Chapter 4

The Model Framework

As a follow-up to the preceding chapter this chapter includes a more thorough analysis of the theory. In the following sections the necessary concepts are introduced and relevant equations and relations are derived. An introductory section discusses the modelling process and aspects of modelling in general.

4.1 Model Building Aspects

Building a model is in general not a straightforward procedure. The methods used will depend on such things as the purpose of the model, the complexity of the system being modelled and what information that can be obtained from the system. However, there are two basic principles when constructing a mathematical model; physical modelling and system identification. In physical modelling the system is divided into subsystems where the behavior of each subsystem is known. This generally means that the physical mechanism applicable to a subsystem can be represented by a set of known equations or otherwise accepted relations. System identification on the other hand is based on observations made from the system. Obtained data is used to adjust model parameters to fit model properties to system properties and in that way reproduce the input-output behavior of the system. Thus the system is modelled without regard to its physical structure. Often models are built combining physical modelling and identification. Mathematical modelling is treated in [3] and some modelling examples can be found in [10].

4.2 Modelling Outline

The objective is to build a real time model of an existing gyroscope. To outline the modelling process a few important conditions must be taken into consideration:

- The real system, i.e. gyroscope and coils, is available for some specific experiments

- The system is relatively non-complex in its physical structure
- The theory describing the physical mechanisms is for the most part well developed and documented
- The real-time demand

The lab bench allowed measurements of certain signals and experiments of system behavior could also be made. With the assist of a GUI (Graphical User Interface) the gyroscope in the missile could be controlled and interesting signals could be monitored and collected. The GUI was used to manoeuvre the gyroscope to desired positions or to keep it locked on a fictive target while the missile was simulating a roll.

The use of the model in a control loop relaxes the demands on it somewhat. Model errors that result in small deviations or slow drifts are reduced by the servomechanism of the control unit. Instead the ability to simulate the behavior of the gyroscope during rapid changes of the reference signal (desired position) will be of primary importance. The performance of the model and its likeness to the real system is measured in terms of tracking velocity.

For a model intended to run as a part of a HWIL simulation there are a few requirements that must be met. Most importantly the model needs to be fast in terms of the number of calculations performed every sample. This puts a restriction on model complexity. In this case the main application allows less than $3 \mu\text{s}$ per time step for the gyro model to compute its output. The current workstation used in the simulations runs in 3 GHz and a crude estimation would be that 10^9 floating point operations is performed every second during the calculation of the model output. That is a maximum of 3000 floating point operations per output sample.

With the conditions in mind, a reasonable approach would be to use physical modelling for most part and to use identification to determine the unknown parameters, i.e. a grey-box model. The model can then be tested for speed and if it is too slow simplifications can be made. The modelling process is shown in Figure 4.1.

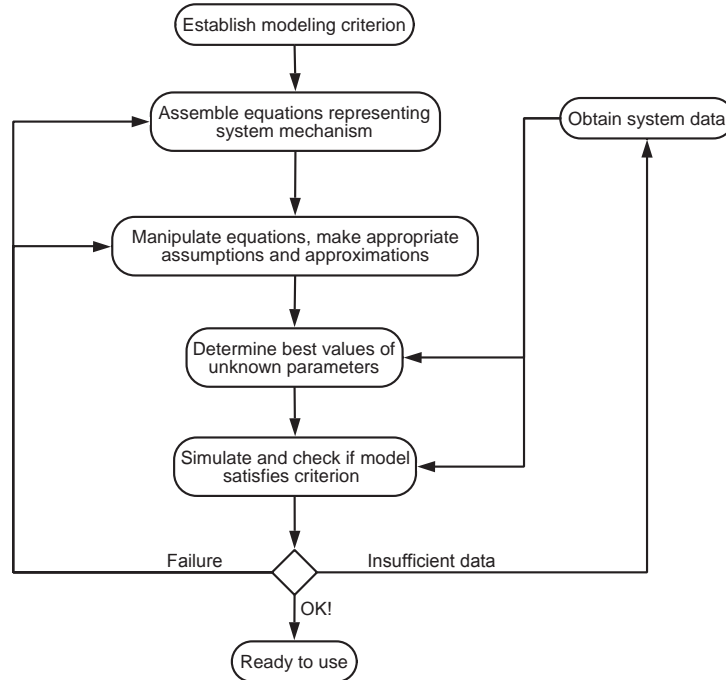


Figure 4.1: The modelling process.

4.3 Representation

A proper representation is important when formulating relations in the model. Here the representation is defined by the reference frames employed and how transformations in these frames are described.

4.3.1 Reference Frames

The description of position and velocity developed in the model depends on the chosen reference frame. Four sets of coordinate frames are introduced:

- **Inertial frame (I)**
A reference frame fixed in space. The inertial frame is considered to coincide with the seeker body frame prior to any rotation.
- **Missile body frame (M)**
A frame fixed in the missile and with its origin at the center of gravity of the seeker. The x-axis is pointing forward out of the nose, the y-axis is pointing out of the right side and the z-axis points downward relative to the missile.
- **Seeker body frame (S)**
A frame with its origin at the center of gravity of the seeker, and rotating

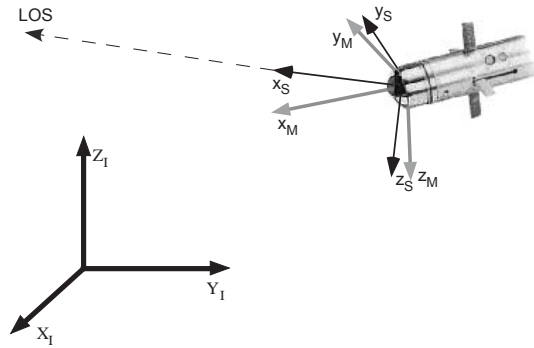


Figure 4.2: The reference frames used in the model.

with the seeker. The axes are defined in the same way as for the missile body frame with the x-axis directed along the seeker LOS, the y-axis pointing to the right and the z-axis pointing downward. The orientation of the seeker relative to the missile is given by the angles pitch and yaw which are described below. Note that there is no rotation about the x-axis and therefore no roll angle.

- **Gyroscope frame (G)**

A frame with its origin at the center of gravity of the gyroscope and with its z-axis directed along the axis of symmetry of the gyroscope. Only the z-axis is embedded in the body and the coordinate axes can rotate with an angular velocity that is different from that of the body.

All frames except the gyroscope frame are drawn in Figure 4.2. The gyroscope frame is explained in Section 4.4.1.

4.3.2 Euler Angles

There are many different representations for describing the rotation of a reference frame relative to another and an independent set of angles may be selected in a variety of ways. The Euler angles are the most common and useful choice. A transformation between two Cartesian coordinate systems is carried out by means of three successive rotations about the x, y or z-axis performed in a specific order. These rotations are always about intermediary axes, i.e. axes in the reference frame that is subject to the rotation. There are several conventions for Euler angles, depending on the axes about which the rotations are carried out and in what order [4]. In this thesis three different representations are employed; the x-convention, yaw-pitch-roll (xyz-convention) and a description using spherical coordinates (angles). The latter would be analogous to a zyx-convention without the last rotation.

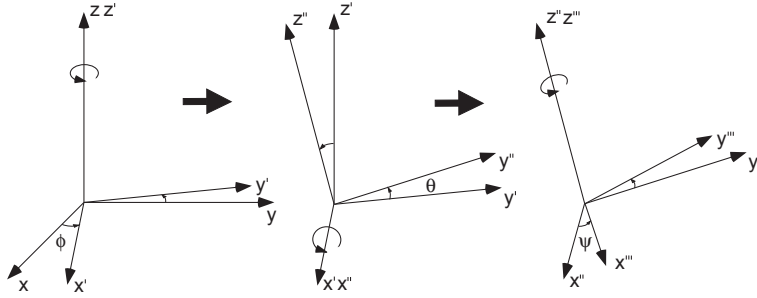


Figure 4.3: Rotation of a reference frame using the x-convention.

x-convention

When using the x-convention the first rotation is by an angle ϕ about the original z-axis, the second is by an angle θ about the x-axis, now pointing in a new direction, and the third is by an angle ψ about the rotated z-axis. This is illustrated in Figure 4.3. Mathematically this sequence of rotations is described by [4]

$$\begin{aligned} & \mathbf{R}_z(\psi) \cdot \mathbf{R}_x(\theta) \cdot \mathbf{R}_z(\phi) = \\ & = \begin{pmatrix} \cos \psi & \sin \psi & 0 \\ -\sin \psi & \cos \psi & 0 \\ 0 & 0 & 1 \end{pmatrix} \cdot \begin{pmatrix} 1 & 0 & 0 \\ 0 & \cos \theta & \sin \theta \\ 0 & -\sin \theta & \cos \theta \end{pmatrix} \cdot \begin{pmatrix} \cos \phi & \sin \phi & 0 \\ -\sin \phi & \cos \phi & 0 \\ 0 & 0 & 1 \end{pmatrix} \end{aligned}$$

The x-convention is used to derive the equations of motion of the gyroscope.

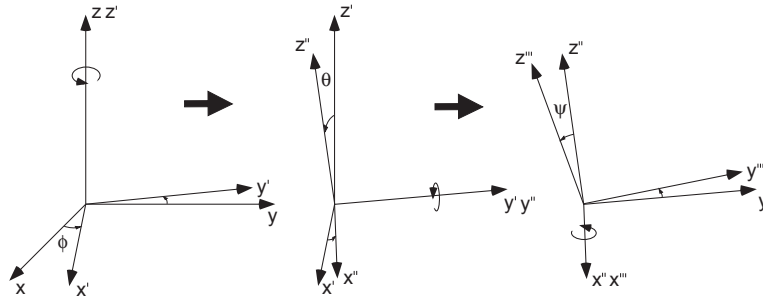


Figure 4.4: Rotation of a reference frame using Yaw-Pitch-Roll.

Yaw-Pitch-Roll

The attitude angles yaw, pitch and roll are a common description of orientation in fields such as aviation, nautics and aeronautics. In classical mechanics this description is referred to as the Euler xyz-convention. The first rotation is by the

angle ϕ_y (yaw) about the z-axis, the second is by the angle θ_p (pitch) about an intermediary y -axis and the last rotation is by the angle ψ_r (roll) about the final x -axis, see Figure 4.4.

The transformation matrix between the inertial frame (I) and the seeker frame (S) is denoted by \mathbf{C}_{IS} and the inverse by \mathbf{C}_{SI} . Hence \mathbf{C}_{IS} describes how the seeker frame is rotated relative to the inertial frame or, equivalently put, it transforms vectors from the I-frame to the S-frame. Since the seeker is bound to rotations about the y - and z -axis, the roll angle ψ_r is omitted. This means that the y -axis always stays in the original (inertial) xy -plane. If subscripts p and y are left out the transformation becomes

$$\begin{aligned} \mathbf{C}_{IS} &= \mathbf{R}_y(\theta) \cdot \mathbf{R}_z(\phi) = \\ &= \begin{pmatrix} \cos \theta & 0 & -\sin \theta \\ 0 & 1 & 0 \\ \sin \theta & 0 & \cos \theta \end{pmatrix} \cdot \begin{pmatrix} \cos \phi & \sin \phi & 0 \\ -\sin \phi & \cos \phi & 0 \\ 0 & 0 & 1 \end{pmatrix} = \\ &= \begin{pmatrix} \cos \phi \cos \theta & \sin \phi \cos \theta & -\sin \theta \\ -\sin \phi & \cos \phi & 0 \\ \cos \phi \sin \theta & \sin \phi \sin \theta & \cos \theta \end{pmatrix} \end{aligned} \quad (4.1)$$

A rotation matrix is orthonormal, which means that the column vectors are mutually orthogonal and the determinant of the matrix is equal to one [2]. An orthonormal matrix satisfies the relation $\mathbf{R}^{-1} = \mathbf{R}^T$, i.e. the inverse of the matrix is identical to the transpose of the matrix. Thus \mathbf{C}_{SI} becomes

$$\mathbf{C}_{SI} = \mathbf{C}_{IS}^T = \begin{pmatrix} \cos \phi \cos \theta & -\sin \phi & \cos \phi \sin \theta \\ \sin \phi \cos \theta & \cos \phi & \sin \phi \sin \theta \\ -\sin \theta & 0 & \cos \theta \end{pmatrix} \quad (4.2)$$

If the rotation of the seeker is relative the missile, i.e. the angles are given relative the M-frame, the transformation matrix and its inverse is denoted as \mathbf{C}_{MS} and \mathbf{C}_{SM} respectively.

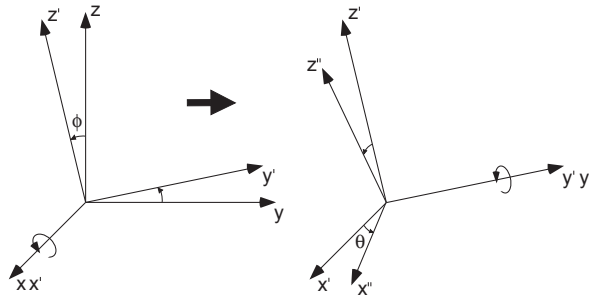


Figure 4.5: Rotation using spherical angles.

Spherical angles

A description in spherical angles is defined by a composition of two rotations; the first is by the angle ϕ_{sph} about the x-axis and second is by the angle θ_{sph} about the rotated y-axis. It is used as an alternative way to describe the direction of the seeker LOS, and for this two angles are adequate. The transformed y- and z-axes are not considered. The transformation vector \mathbf{d}_{xIS} is obtained from the transformation matrix \mathbf{D} according to (again subscripts are left out)

$$\begin{aligned}
 \mathbf{D} &= \mathbf{R}_y(\theta) \cdot \mathbf{R}_x(\phi) = \\
 &= \begin{pmatrix} \cos \theta & 0 & -\sin \theta \\ 0 & 1 & 0 \\ \sin \theta & 0 & \cos \theta \end{pmatrix} \cdot \begin{pmatrix} 1 & 0 & 0 \\ 0 & \cos \phi & \sin \phi \\ 0 & -\sin \phi & \cos \phi \end{pmatrix} = \\
 &= \begin{pmatrix} \cos \theta & \sin \phi \sin \theta & -\cos \phi \sin \theta \\ 0 & \cos \phi & \sin \phi \\ \sin \theta & -\sin \phi \cos \theta & \cos \phi \cos \theta \end{pmatrix} \Rightarrow \\
 &\Rightarrow \mathbf{d}_{xIS}^T = \begin{pmatrix} \cos \theta \\ \sin \phi \sin \theta \\ -\cos \phi \sin \theta \end{pmatrix} \tag{4.3}
 \end{aligned}$$

The latter representation is natural when describing the motion of the gyro during a missile roll and is used by modules outside the gyro model. The rotations are shown in Figure 4.5.

If the elements in (4.2) are known the position of the seeker can be calculated. Use $(c_{11} \ c_{21} \ c_{31})^T$ to denote the first column of (4.2). Then the desired angles can be obtained through

$$\begin{aligned}
 \phi_y &= \arctan \left(\frac{c_{21}}{c_{11}} \right) \\
 \theta_p &= \arctan \left(-\frac{c_{31}}{\sqrt{1 - c_{31}^2}} \right) \tag{4.4}
 \end{aligned}$$

In the calculation of θ_p arctan is preferred over arcsin since it is defined for all real values and arcsin is not.

Furthermore, identification of the elements in (4.1) and (4.3) gives the transformation between the representations yaw-pitch and spherical angles

$$\begin{aligned}
 \phi_y &= \arctan (\tan \theta_{sph} \sin \phi_{sph}) \\
 \theta_p &= \arcsin (\sin \theta_{sph} \cos \phi_{sph}), \quad -\frac{\pi}{2} < \theta_p < \frac{\pi}{2} \tag{4.5}
 \end{aligned}$$

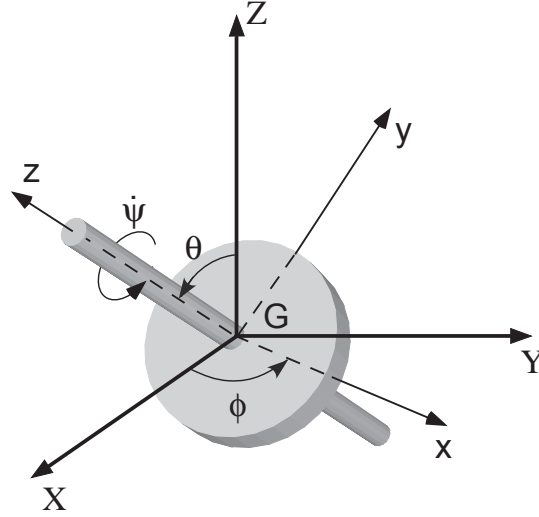


Figure 4.6: The gyroscope reference frame.

and

$$\begin{aligned}\theta_{sph} &= \arccos(\cos \theta_p \cos \phi_y) \\ \phi_{sph} &= \arctan 2\left(\frac{\sin \phi_y}{\tan \theta_p}\right), \quad 0 \leq \phi_{sph} \leq 2\pi\end{aligned}\tag{4.6}$$

4.4 System Dynamics

The moving part of the gyro system is the gyroscope (see Section 3.3). The motion of gyroscopes is often treated as a special case of general motion of rigid bodies. Gyroscopic motion occurs when the axis about which a body is spinning is itself rotating about an axis. Common examples of this are the motions of a spinning top or that of gyroscopes in inertial guidance systems. In these applications the body is axisymmetric and is spinning about its axis of symmetry. Gyroscopes are treated in most books on dynamics, see for example [13], [9] or [2].

4.4.1 Equations of Motion

The equations describing the motion of an axisymmetric body are derived from the general angular-momentum equations. The gyroscope frame introduced in Section 4.3 is a natural choice of coordinates for this problem, see Figure 4.6. The axisymmetrical body is rotating about its center of mass G , with the axis of symmetry along the z -axis. This makes the x - and y -axes automatically principal axes of inertia along with the z -axis [13]. The X - Y - Z axes are fixed in space. To describe the motion the Euler x -convention introduced in Section 4.3.2 is used. θ

measures the inclination of the rotor axis from the Z-axis and is called the nutation angle. The x-axis always remains in the XY-plane and the angle ϕ between the X- and x-axes is called the precession angle. The spin velocity is represented by $\dot{\psi}$. Note that x-y-z does not constitute a body frame since x and y are not attached to the body [13]. From Figure 4.6. the components of the angular velocity $\boldsymbol{\Omega}$ of the x-y-z axes and the angular velocity $\boldsymbol{\omega}$ of the rotor can be deduced [13], [9]

$$\begin{aligned}\Omega_x &= \dot{\theta} \\ \Omega_y &= \dot{\phi} \sin \theta \\ \Omega_z &= \dot{\phi} \cos \theta\end{aligned}\quad (4.7)$$

and

$$\begin{aligned}\omega_x &= \dot{\theta} \\ \omega_y &= \dot{\phi} \sin \theta \\ \omega_z &= \dot{\phi} \cos \theta + \dot{\psi}\end{aligned}\quad (4.8)$$

The axes and the body have identical x- and y-components of angular velocity while the z-component differs by the relative angular velocity $\dot{\psi}$.

The general angular-momentum equation for a system with constant mass in a rotating reference frame with angular velocity $\boldsymbol{\Omega}$ is [13]

$$\sum \mathbf{M} = \left(\frac{d\mathbf{H}}{dt} \right)_{xyz} + \boldsymbol{\Omega} \times \mathbf{H} \quad (4.9)$$

where \mathbf{M} is the external torque and \mathbf{H} is the angular momentum.

Furthermore, for a body with angular velocity $\boldsymbol{\omega}$ and inertia tensor \mathbf{I} the expression for \mathbf{H} about its mass center G can be written as a matrix product [13]

$$\mathbf{H} = \mathbf{I}\boldsymbol{\omega} \quad (4.10)$$

Since the x-y-z-axes are principal axes of inertia the inertia tensor \mathbf{I} is diagonalized. Also, due to symmetry I_{xx} and I_{yy} are identical. The tensor is written

$$\mathbf{I} = \begin{pmatrix} I_0 & 0 & 0 \\ 0 & I_0 & 0 \\ 0 & 0 & I \end{pmatrix}$$

Where $I_0 = I_{xx} = I_{yy}$ and $I = I_{zz}$. By substituting $\boldsymbol{\omega}$ and $\boldsymbol{\Omega}$ in (4.9) and (4.10) with their components (4.7) and (4.8) and then using (4.10) in (4.9) the final equations of motion can be stated

$$\begin{aligned}\sum M_x &= I_0 \left(\ddot{\theta} - \dot{\phi}^2 \sin \theta \cos \theta \right) + I \dot{\phi} \left(\dot{\phi} \cos \theta + \dot{\psi} \right) \sin \theta \\ \sum M_y &= I_0 \left(\ddot{\phi} \sin \theta + 2\dot{\phi}\dot{\theta} \cos \theta \right) - I \dot{\theta} \left(\dot{\phi} \cos \theta + \dot{\psi} \right) \\ \sum M_z &= I \frac{d}{dt} \left(\dot{\phi} \cos \theta + \dot{\psi} \right)\end{aligned}\quad (4.11)$$

In a given problem, the solution will depend in the sum of torques applied to the body about the three coordinate axes.

4.4.2 Steady Precession

The equations stated above are general for a symmetrical body rotating about either a fixed point or the mass center and could be used as they are in a given problem. However, solving these equations is not easily done and would require cumbersome computations. To simplify this matter a common assumption can be made. Here the body is spinning about its axis of symmetry at constant velocity and precesses around another axis at a steady rate. This means that $\dot{\psi}$, $\dot{\phi}$ and θ are constants. This special case is called steady precession. The equations (4.11) simplifies to

$$\begin{aligned}\sum M_x &= \dot{\phi} \sin \theta \left[I \left(\dot{\phi} \cos \theta + \dot{\psi} \right) - I_0 \dot{\phi} \cos \theta \right] \\ \sum M_y &= 0 \\ \sum M_z &= 0\end{aligned}\tag{4.12}$$

By examining the equations a few comments can be made. For a gyroscope to undergo steady state precession the forces acting upon it must provide a constant torque about the x-axis. This means that the torque axis is perpendicular to both the precession axis (Z-axis) and the spin axis (z-axis).

To simplify things even further, consider the case when the precession axis is perpendicular to the spin axis as seen in Figure 4.7. With $\theta = \pi/2$, (4.12) becomes

$$\sum M_x = I \dot{\phi} \dot{\psi}\tag{4.13}$$

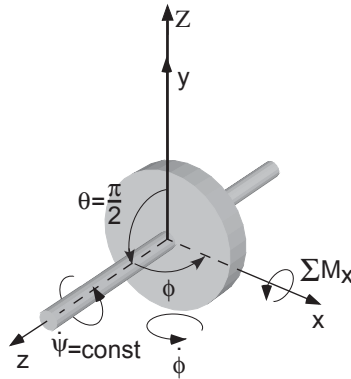


Figure 4.7: The special case where the precession axis is perpendicular to the spin axis.

4.5 Electromagnetics

Electromagnetic theory must be used to describe the behavior of the system and the forces that are involved controlling the gyroscope. As was described in Chapter 3, this system consists mainly of two parts; the magnetic gyroscope and the coils surrounding it. While the previous section discussed the dynamical aspect of the gyro system the following text will focus on its electromagnetic properties.

4.5.1 Magnetic Dipole Moment

The magnetic property of a permanent magnet is determined by the magnetic dipole moment \mathbf{m} of the material. In a traditional bar magnet this vector is directed from the south to the north pole and creates a magnetic field outside and inside the magnet. The magnetic moment in materials arises from the individual magnetic moments of the atoms [1]. In a permanent magnet they are (approximately) aligned in a certain direction and this creates a total magnetic dipole moment and thereby net magnetism. Assuming that the individual dipole moments \mathbf{m}_i of the atoms are perfectly aligned the total dipole moment \mathbf{m} is

$$\mathbf{m} = n\mathbf{m}_i \quad (4.14)$$

where n is the number of atoms in the magnet.

(4.14) is thus an alternative way of writing (3.1). This accounts for any ordinary permanent magnet no matter shape. For ferromagnetic materials the magnetic moment per atom can be found in tables such as [11]. The cylindrical shaped magnet in the gyroscope along with its magnetic dipole moment is illustrated in Figure 4.8. For a better understanding of how the direction of the magnetic moment is determined the magnet can be viewed as a constitution of small (or even atomic) bar magnets [1].

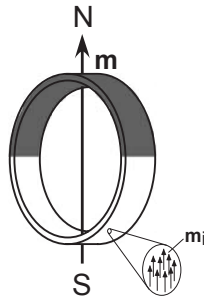


Figure 4.8: The circular shaped magnet with the magnetic dipole moment \mathbf{m} .

4.5.2 Magnetic Fields

The magnetic field is created by running an electric current through the coils surrounding the gyroscope. It is desirable to derive an expression of how this magnetic field varies throughout the volume around the coils and to sort out the dependency on such things as geometry and the location of the coils. Since orientations are given relative to the x-y-z axes, the magnetic fields will be derived using Cartesian coordinates. There are two pairs of coils that have to be considered; the precession coils and the spin coils.

The Single Closed Loop

The magnetic field created by the precession coils is calculated by first considering the case of a single closed loop. In a single closed loop the magnetic field caused by a current can be determined by using the Biot-Savart law [1]

$$\mathbf{B}(t) = \frac{\mu_0 i(t)}{4\pi} \int_C \frac{d\ell \times \hat{\mathbf{e}}_r}{r^2} \quad (4.15)$$

Here C is the closed loop with radius R conducting the current $i(t)$. $\hat{\mathbf{e}}_r$ is the unit vector directed from the source point $d\ell$ to the field point and r is the distance between the points. μ_0 is the permeability of free space. This is depicted in Figure 4.9. Also shown in the figure is the distance $r_{//}$ and the angles ϕ and ψ . $r_{//}$ denotes the length of the projection of $r\hat{\mathbf{e}}_r$ in the YZ-plane and ψ is the angle measured between $\hat{\mathbf{e}}_r$ and the YZ-plane. From inspection of the figure the distance r and the source point element $d\ell$ can be expressed using ϕ according to

$$r^2 = r_{//}^2 + x^2 = (R \sin \phi - z)^2 + (R \cos \phi)^2 + x^2 \quad (4.16)$$

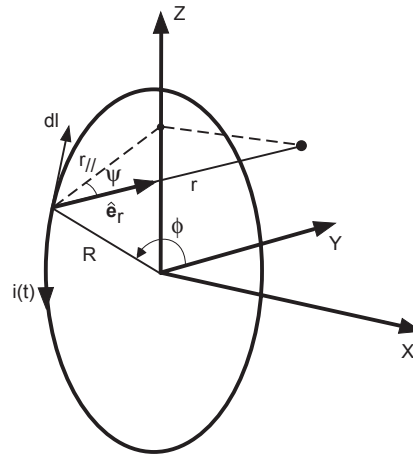


Figure 4.9: The circular loop carrying the current $i(t)$.

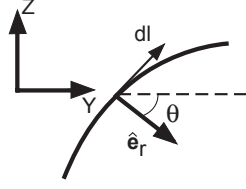


Figure 4.10: The loop projected onto the YZ-plane.

and

$$d\ell = \begin{pmatrix} 0 \\ R \sin \phi \, d\phi \\ -R \cos \phi \, d\phi \end{pmatrix} \quad (4.17)$$

The unit vector $\hat{\mathbf{e}}_r$ can be expressed in Cartesian coordinates by introducing a third angle θ as shown in Figure 4.10. Inspection of Figures (4.9) and (4.10) yields

$$\hat{\mathbf{e}}_r = \begin{pmatrix} \sin \psi \\ \cos \theta \cos \psi \\ \sin \theta \cos \psi \end{pmatrix} \quad (4.18)$$

Furthermore, the angles ψ and θ can be expressed as

$$\begin{aligned} \psi &= \arctan\left(\frac{x}{r_{//}}\right) \\ \theta &= \arctan\left(\frac{R \sin \phi - z}{R \cos \phi}\right) \end{aligned} \quad (4.19)$$

This is convenient because now the final integration can be made over the single variable ϕ . Substituting θ and ψ in (4.18) with (4.19) and using the Biot-Savart law (4.15) with (4.16) and (4.17) inserted the magnetic field becomes

$$\mathbf{B}(t) = \frac{\mu_0 i(t)}{4\pi} \int_0^{2\pi} \frac{1}{(R^2 + z^2 - 2zR \sin \phi + x^2)^{\frac{3}{2}}} \begin{pmatrix} zR(\sin \phi - R) \\ -xR \cos \phi \\ -xR \sin \phi \end{pmatrix} d\phi \quad (4.20)$$

Here the final expression is obtained by using an algebraic solver. This integral only have an analytical solution in the y-direction [12]. For a complete solution numerical methods are used.

4.5.3 Magnetic Torque

A magnet put in an external magnetic field will experience a force that tends to rotate it in such a way as to align the magnetic dipole moment vector with the magnetic field. The torque \mathbf{M} about the point of rotation is given by the relation [1]

$$\mathbf{M} = \mathbf{m} \times \mathbf{B} \quad (4.21)$$

Here \mathbf{m} is the magnetic dipole moment of the magnet and \mathbf{B} is a uniform magnetic field. From this equation it follows that the exerted torque decreases as the magnet is rotated and vanish when the magnetic dipole moment is parallel to the magnetic field.

In the seeker the magnetic field is not uniform and to find the total torque \mathbf{M} acting on the magnet, consider a torque \mathbf{M}_i calculated for every point in the magnet. The total torque is obtained from the sum

$$\mathbf{M} = \sum_{i=1}^n \mathbf{M}_i = \sum_{i=1}^n (\mathbf{m}_i \times \mathbf{B}_i) \quad (4.22)$$

The number of points n will actually be the number of atoms in the magnet. From linear algebra the following identities can be obtained [5]

$$\mathbf{a} \times (\mathbf{b} + \mathbf{c}) = \mathbf{a} \times \mathbf{b} + \mathbf{a} \times \mathbf{c} \quad (4.23)$$

$$(\lambda \mathbf{a}) \times \mathbf{b} = \mathbf{a} \times (\lambda \mathbf{b}) = \lambda(\mathbf{a} \times \mathbf{b}) \quad (4.24)$$

Under the assumption that all \mathbf{m}_i are aligned and thus identical (4.22) can be expanded using (4.23) and (4.24)

$$\sum_{i=1}^n (\mathbf{m}_i \times \mathbf{B}_i) = \mathbf{m}_i \times \sum_{i=1}^n \mathbf{B}_i = (n\mathbf{m}_i) \times \left(\frac{1}{n} \sum_{i=1}^n \mathbf{B}_i \right) \quad (4.25)$$

Observing that right hand summation in (4.25) is an average of \mathbf{B} and by using (4.14) the torque can be calculated according to the relation

$$\mathbf{M} = \mathbf{m} \times \mathbf{B}_{average} \quad (4.26)$$

This shows that the torques $\mathbf{M}_1, \mathbf{M}_2, \dots, \mathbf{M}_i$ does not have to be considered, instead the average magnetic field taken over the magnet can be used to calculate the total torque acting on the gyroscope.

Chapter 5

Model Construction

The previous chapter introduced the theory central to the model and a framework was presented. In this chapter the equations and expressions derived are used to form a complete model of the gyro system. The real system is investigated in detail in order to further develop the expressions and to be able to make appropriate assumptions and approximations.

5.1 Dynamics

In Section 4.4.2 the necessary conditions for steady state precession was stated. Considering these conditions it is a special case that is somewhat theoretic in nature. In real life applications the moment can only be arbitrary close to constant for example. Also if the transition from initial state should be considered the use of (4.12) or (4.13) is not obvious. Still a lot of engineering applications involving gyroscopic motion is very well described by steady state. The question is how good this assumption is when looking at the problem at hand.

5.1.1 Steady State Approximation

The basic idea behind controlling the gyroscope in the missile is to apply a force and a resulting torque that makes the gyroscope precess in a certain direction. It is shown later in this section that the applied torque is nearly perpendicular to the spin axis of the gyroscope. By assuming that the motion can be described as steady state precession and that the precession occurs around an axis perpendicular to the spin axis (4.13) can be used instead of (4.11). The approximation introduces an error in the model that will depend on the applied torque, initial conditions and the inertial properties of the gyroscope. If the approximation is too crude simulations will likely show poor results regardless of how the other parts are modelled. Hence, to support the use of (4.13), a simple case is considered. The motion is calculated using both the approximate and the exact description and results are compared.

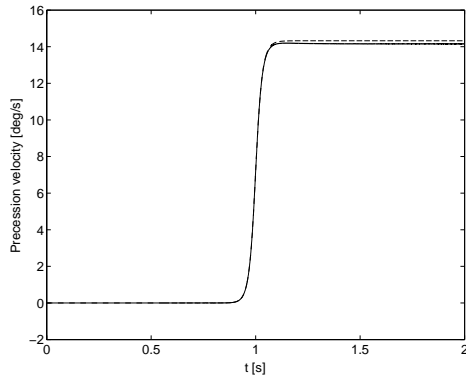


Figure 5.1: Precession velocity $\dot{\phi}$ using steady state approximation (dashed) and exact solution (solid)

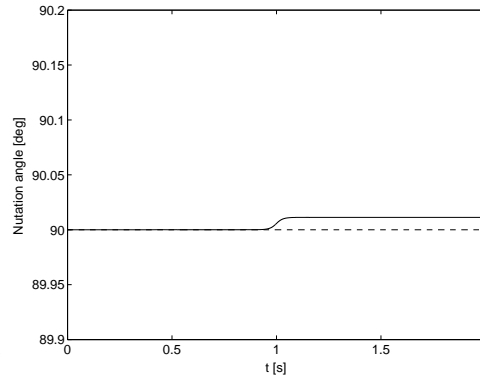


Figure 5.2: Nutation angle θ using steady state approximation (dashed) and exact solution (solid).

A typical situation is where the gyroscope is set to move from its initial position to a new position tracing a target. In the extreme case the gyroscope is taken from rest to its maximum velocity in an instance. This can be simulated by applying a step-like torque and setting the initial value of the precession velocity $\dot{\phi}$ to 0. Initial values of spin velocity $\dot{\psi}$ and nutation angle θ is set to $2\pi \cdot 100$ and $\pi/2$ respectively. The moments of inertia of the gyroscope, I and I_0 , are estimated as described in Section 5.4. The components of the simulated torque is

$$\begin{aligned} M_x &= M_0 \arctan(t^{50}) \\ M_y &= 0 \end{aligned} \quad (5.1)$$

$$M_z = M_0 \sin(\alpha) \arctan(t^{50}) - M_f(\dot{\psi}) \quad (5.2)$$

The magnitude M_0 is determined knowing the maximum angular velocity of the gyroscope. The torque along the z-axis is non-zero for cases where $\theta_{sph} \neq 0$, i.e. the gyroscope is rotated relative the missile. α is set to a value corresponding to the maximum rotation. The term $M_f(\dot{\psi})$ is a simple model of the friction (linear in $\dot{\psi}$) and can be estimated from observations of the real gyroscope.

Figures 5.1 and 5.2 shows the change in $\dot{\phi}$ and θ when the step-like torque is applied. Viewing the plots it is apparent that the difference in precession velocity is very small between the solutions and that the nutation (change in θ) is negligible. Although this case is a construct it clearly indicates that the motion of the gyroscope is approximately steady state precession.

To be used in the model (4.13) is first expressed in the seeker frame of reference

$$M_y = I\Omega_z p_x \quad (5.3)$$

where Ω_z is the precession velocity along the z-axis, and p_x is the spin velocity directed along the x-axis (the seeker LOS). The torque M_y is perpendicular to Ω_z

and p_x . This equation can be generalized to include precession about any axis perpendicular to the spin axis. Due to symmetry and the fact that vectors M_y , Ω_z and p_x are mutually perpendicular the equation can be written in the cross-product form

$$\mathbf{M} = I\boldsymbol{\Omega} \times \mathbf{p} \quad (5.4)$$

This form is used in [9].

(5.4) can be used to describe the motion of the gyroscope in terms of precession velocity. Furthermore, according to (4.26) the torque is determined by the applied magnetic field \mathbf{B} and the magnetic dipole moment \mathbf{m} of the magnet. The precession velocity of the gyroscope can thus be expressed as a function of \mathbf{B} and \mathbf{m} by combining (4.26) and (5.4)

$$\begin{aligned} \mathbf{m} \times \mathbf{B} &= I\boldsymbol{\Omega} \times \mathbf{p} \Rightarrow \\ \Rightarrow \begin{pmatrix} 0 \\ m_y \\ m_z \end{pmatrix} \times \begin{pmatrix} B_x \\ B_y \\ B_z \end{pmatrix} &= I \begin{pmatrix} \Omega_x \\ \Omega_y \\ \Omega_z \end{pmatrix} \times \begin{pmatrix} p_x \\ 0 \\ 0 \end{pmatrix} \Rightarrow \\ \Rightarrow \begin{pmatrix} m_y B_z - m_z B_y \\ m_z B_x \\ -m_y B_x \end{pmatrix} &= I \begin{pmatrix} 0 \\ \Omega_z p_x \\ -\Omega_y p_x \end{pmatrix} \end{aligned} \quad (5.5)$$

It is seen that torque directed along the x-axis does not contribute to the precession velocity. This is expected since the precession arises from torques acting perpendicular to the rotation axis. Still, a torque along the x-axis will be equivalent to an angular acceleration of the rotor and thereby affect the total motion of the gyroscope.

The magnetic field in (5.5) is given in missile coordinates and must be transformed to the seeker reference frame. If the attitude of the missile is given in angles roll, pitch and yaw relative to the inertial reference frame, the seeker position relative to the missile simply becomes

$$\theta_p = \theta_p^{seeker} - \theta_p^{missile} \quad (5.6)$$

$$\phi_y = \phi_y^{seeker} - \phi_y^{missile} \quad (5.7)$$

Because of the symmetry the roll angle does not have to be considered.

(5.6) and (5.7) can be inserted into the transformation matrix (4.1) to give the magnetic field in the seeker reference according to

$$\mathbf{B}_S = \mathbf{C}_{MS}\mathbf{B}_M = \begin{pmatrix} B'_x \cos \phi_y \cos \theta_p + B'_y \sin \phi_y \cos \theta_p - B'_z \sin \theta_p \\ -B'_x \sin \phi_y + B'_y \cos \phi_y \\ B'_x \cos \phi_y \sin \theta_p + B'_y \sin \phi_y \sin \theta_p + B'_z \cos \theta_p \end{pmatrix} \quad (5.8)$$

where B'_x , B'_y and B'_z denotes the magnetic field components in the M-frame.

Since the angles are relative the missile reference frame the transformation matrix is denoted as \mathbf{C}_{MS} , i.e. transformation from the M-frame to the S-frame (see Section 4.3.2).

Assuming that B'_x is the dominating term, (5.8) shows that the y- and z-components of the magnetic field relative the seeker is small for small rotations (θ_p and ϕ_y small). The torque acting on the gyroscope can be considered approximately perpendicular to the spin-axis in the range specified ($\theta_{sph} < 15$ degrees). Ignoring the right hand side x-component in (5.5) an solving for $\boldsymbol{\Omega}$ will lead to an expression for the precession velocity of the gyroscope in the seeker body frame

$$\boldsymbol{\Omega}_{prec} = \begin{pmatrix} \Omega_x \\ \Omega_y \\ \Omega_z \end{pmatrix} = \begin{pmatrix} 0 \\ m_z B_x / I p_x \\ m_y B_x / I p_x \end{pmatrix} \quad (5.9)$$

Considering the discussion above B_x decreases when θ_{sph} increases and in view of (5.9) the performance of the seeker in terms of maximum angular velocity is thus expected to deteriorate slightly for wide angles.

The magnetic dipole moment vector \mathbf{m} rotates in the seeker yz-plane since the magnet is attached to the gyroscope. Hence, in the seeker frame \mathbf{m} becomes

$$\mathbf{m} = \begin{pmatrix} 0 \\ m_y \\ m_z \end{pmatrix} = \begin{pmatrix} 0 \\ m \cos(\omega_{ref} t) \\ m \sin(\omega_{ref} t) \end{pmatrix} \quad (5.10)$$

where $\omega_{ref} = 2\pi \cdot p_x$.

In this thesis p_x is considered to be constant in (5.9). This is an approximation but will not affect the results considerably. However, in cases where the model is fed with the same control signals as the real system it is important that the spin-rate matches the spin-rate of the seeker. Then ω_{ref} is measured and input to the model along with the control signal ($p_x \approx \omega_{ref} / 2\pi$).

5.2 The State Space Description

Since the seeker is confined to angular motion about its y- and z-axis only, the angular velocity of the seeker is equal to the precession velocity of the gyroscope. Thus

$$\boldsymbol{\Omega}_S = \boldsymbol{\Omega}_{prec} \quad (5.11)$$

$\boldsymbol{\Omega}_S$ is used to update the position of the seeker, but since the position is given relative to the inertial frame, $\boldsymbol{\Omega}_S$ must be transformed to this frame of reference. This is done by using the inverse of \mathbf{C}_{IS} given by (4.2).

$$\boldsymbol{\Omega}_I = \mathbf{C}_{SI} \cdot \boldsymbol{\Omega}_S = \begin{pmatrix} \Omega'_x \\ \Omega'_y \\ \Omega'_z \end{pmatrix} \quad (5.12)$$

The position of the seeker is described by (4.1), and to find the differential equation, an expression for the time derivative must be derived. The time derivative

$$\dot{\mathbf{C}}_{SI} = \frac{d}{dt} \mathbf{C}_{SI} \quad (5.13)$$

is equivalent to a differentiation of the column vectors. In \mathbf{C}_{SI} these are the unit vectors of the S-frame represented in the I-frame. Furthermore, the time differentials in the seeker frame and inertial frame can be related through [9], [13], [2]

$$\left. \frac{d\hat{\mathbf{e}}_i}{dt} \right|_I = \left. \frac{d\hat{\mathbf{e}}_i}{dt} \right|_S + \boldsymbol{\Omega}_I \times \hat{\mathbf{e}}_i \quad i = 1, 2, 3 \quad (5.14)$$

Where $\hat{\mathbf{e}}_i$ denotes a unit vector along the x-axis, the y-axis or the z-axis in the S-frame. Since the unit vectors are fixed in their reference frame by definition, the relation (5.14) can be written

$$\left. \frac{d\hat{\mathbf{e}}_i}{dt} \right|_S = 0 \quad \Rightarrow \quad \left. \frac{d\hat{\mathbf{e}}_i}{dt} \right|_I = \boldsymbol{\Omega}_I \times \hat{\mathbf{e}}_i \quad i = 1, 2, 3 \quad (5.15)$$

This relation shows that $\dot{\mathbf{C}}_{SI}$ can be factorized according to

$$\dot{\mathbf{C}}_{SI} = \begin{pmatrix} 0 & -\Omega'_z & \Omega'_y \\ \Omega'_z & 0 & -\Omega'_x \\ -\Omega'_y & \Omega'_x & 0 \end{pmatrix} \cdot \mathbf{C}_{SI} \quad (5.16)$$

The skew-symmetric matrix

$$\mathbf{C}_\Omega = \begin{pmatrix} 0 & -\Omega'_z & \Omega'_y \\ \Omega'_z & 0 & -\Omega'_x \\ -\Omega'_y & \Omega'_x & 0 \end{pmatrix} \quad (5.17)$$

is referred to as the angular velocity matrix and has the same elements as the angular velocity vector $\boldsymbol{\Omega}_I$.

(5.16) is used to update the position of the seeker. Since only the x-axis is of interest the state vector $\mathbf{x}(t) = \hat{\mathbf{e}}_1$ is introduced. $\hat{\mathbf{e}}_1$ is the unit vector along the x-axis, i.e. the first column of \mathbf{C}_{SI} . The state space description becomes

$$\begin{aligned} \dot{\mathbf{x}}(t) &= \mathbf{C}_\Omega \mathbf{x}(t) \\ y_1(t) &= \arctan \left(\frac{x_2(t)}{x_1(t)} \right) \\ y_2(t) &= \arctan \left(-\frac{x_3(t)}{\sqrt{1 - x_3^2(t)}} \right) \end{aligned} \quad (5.18)$$

Here the output signals $y_1(t)$ and $y_2(t)$ are the angles ϕ_y and θ_p calculated using (4.4). The input signal (referred to as $u(t)$ in Figure 3.1) is contained in (5.17) since the angular velocity (5.9) is a function of B_x (which is proportional to the input of the system).

5.2.1 Position Update Approximation

To update the position using the state space description given by (5.18) a matrix operation and two trigonometric calculations are required (if not including (5.12)). Considering that the model have limited processor time an alternative approximative position update is introduced.

Angular velocity is by definition the rate of change of a rotation. A natural approximation is therefore to update the angles ϕ_y , θ_p and thus the position, by integration of the angular velocity $\mathbf{\Omega}_I$, that is,

$$\begin{aligned}\theta_p &\approx \int \Omega'_y dt \\ \phi_y &\approx \int \Omega'_z dt\end{aligned}\tag{5.19}$$

Since angular velocity is a vector quantity and rotations (angles) are not (5.19) only give the correct position for certain special cases. However, it is still a good approximation for small rotations. This follows from the fact that discrepancies between spatial rotations that differ only in their sequence become less significant as the magnitude of each rotation decreases (for infinitesimal rotations a composite rotation is independent of the sequence). See [2] for details on infinitesimal rotation and angular velocities.

The approximation is feasible since the rotation of the seeker is limited to about 15

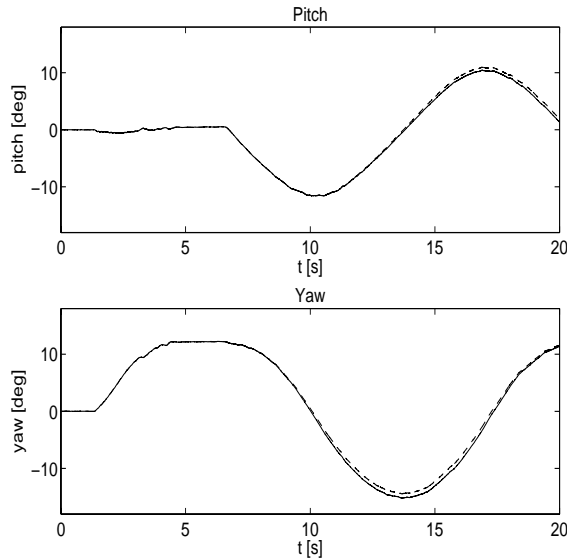


Figure 5.3: Simulation output using approximative position update (dashed) and state space description (solid).

degrees in one direction. No mathematical theory is developed, instead appropriate test runs with the approximative update (5.19) and the state space description (5.18) are compared. The plots in Figure 5.3 shows the output from a simulation where the rotation is near maximum. During this simulation the difference is less than 0.8 degrees which can be considered acceptable. The error is expected to grow with time, however this will not be critical when the model is used in the application (see Section 6.2). Note that the solutions are identical during the first rotation about the z-axis. This is the case for any single rotation about one of the coordinate axes.

5.3 Modelling the Coils

The precession coils and the spin coils described in Section 3.4 must be modelled in order to simulate the motion of the gyroscope. While the magnetic field generated by the precession coils creates the torque that in the end controls the gyroscope the effects from the spin coils can be considered as disturbances in the system.

5.3.1 The Spin Coils

The HWIL simulator uses a set of spin coils to keep the gyroscope at a steady spin-rate during simulation. The system consisting of stationary wire windings and a rotating magnet is equivalent to an AC motor. In the simplest case the motor consist of one pair of coils on either side of the magnetic rotor [6]. Consider a similar assembly in the missile/launch tube. The magnetic field that arises from the coils will be parallel to the missile yz-plane. Prior to launch the seeker is locked in the center and $\theta_{sph} = 0$, i.e. the seeker LOS is directed along the missile x-axis. The dipole moment vector of the magnet (5.10) thus rotates in the yz-plane. According to (4.21) the torque is then directed along the x-axis and the resulting angular velocity (spin-rate) ω of the magnetic gyroscope can be determined by

$$M_x - M_f(\omega) = I\dot{\omega} \quad (5.20)$$

where $M_f(\omega)$ is a friction term due to the rotation.

From experience, i.e. through observations, the locked gyro will have a spin-rate that is close to constant and any effort put in modelling the spin coils would thus be unjustified. However, the model of the gyroscope is run in the HWIL environment and during simulation $\theta_{sph} \neq 0$ in general. This complicates matters somewhat. Now the torque is no longer directed along the spin-axis and the motion of the gyroscope will not be bound to the plane motion given by (5.20). Instead the magnetic field will affect the precession velocity of the gyroscope and the spin coils must be included in the model along with the precession coils. Since there is no description of the spin coils available, a heuristic approach is employed combining physical modelling and system identification as described in Section 4.1.

Considering the discussion above a simple model would be a uniform time-varying magnetic field perpendicular to the x-axis. In the M-frame this magnetic

field can be written

$$\mathbf{B} = \begin{pmatrix} 0 \\ B'_y \\ B'_z \end{pmatrix} = \begin{pmatrix} 0 \\ B_{y0} \sin(\omega_y t + \varphi_y) \\ B_{z0} \sin(\omega_z t + \varphi_z) \end{pmatrix} \quad (5.21)$$

where B_{y0} and B_{z0} are positive constants.

To study the effects of (5.21) on the gyroscope it is transformed to the S-frame x-component using (4.3) (treating the M-frame as the inertial frame)

$$B_x = \mathbf{d}_{xMS} \mathbf{B} = B'_y \sin \phi \sin \theta - B'_z \cos \phi \sin \theta \quad (5.22)$$

As in (4.3) $\theta = \theta_{sph}$ and $\phi = \phi_{sph}$.

The change in position over a time period T ($\Delta\theta_p$, $\Delta\phi_y$) is approximated by (5.19) to be

$$\Delta\theta_p \approx \widehat{\Delta\theta_p} = \int_0^T \Omega_y dt = C \int_0^T B_x \cos(\omega_{ref} t) dt \quad (5.23)$$

$$\Delta\phi_y \approx \widehat{\Delta\phi_y} = \int_0^T \Omega_z dt = C \int_0^T B_x \sin(\omega_{ref} t) dt \quad (5.24)$$

where $T = 2\pi/\omega_{ref}$, C is a constant and B_x is the S-frame x-component of \mathbf{B} . The components of \mathbf{m} is substituted using (5.10). Using (5.22) B_x can be expressed as

$$\begin{aligned} B_x &= B_{y0} \sin(\omega_y t + \varphi_y) \sin \phi \sin \theta - B_{z0} \sin(\omega_z t + \varphi_z) \cos \phi \sin \theta = \\ &= f(\phi, \theta) \sin(\omega_y t + \varphi_y) + g(\phi, \theta) \sin(\omega_z t + \varphi_z) \end{aligned} \quad (5.25)$$

where

$$f(\phi, \theta) = B_{y0} \sin \theta \sin \phi \quad (5.26)$$

$$g(\phi, \theta) = -B_{z0} \sin \theta \cos \phi \quad (5.27)$$

If (5.21) is correct modelling the spin coils comes down to determining the parameters B_{y0} , ω_y , φ_y , B_{z0} , ω_z and φ_z .

ω_y and ω_z can be deduced immediately. As for the AC motor the frequency of the varying magnetic field must be equal to the spin-rate of the magnet (see for example [1]), thus

$$\omega_y = \omega_z = \omega_{ref} \quad (5.28)$$

The phases φ_y and φ_z depends on the number of coil pairs and their placement. Consider two cases:

Case 1

In the first case only one pair of coils is used. Then there is one source and $\varphi_y = \varphi_z = \varphi$. Assuming that the magnetic field is in phase with the rotating magnet this will be equivalent to placing the coils on an axis in yz-plane rotated

an angle $\phi = -\varphi$ measured from the z-axis. This case is depicted in Figure 5.4(a). Using (5.28) in (5.25), (5.23) and (5.24) becomes

$$\begin{aligned}\widehat{\Delta\theta}_p &= C(f(\phi, \theta) + g(\phi, \theta)) \int_0^T \sin(\omega_{ref}t + \varphi) \cos(\omega_{ref}t) dt = \\ &= C(f(\phi, \theta) + g(\phi, \theta)) \int_0^T \frac{1}{2}(\sin(2\omega_{ref}t + \varphi) + \sin \varphi) dt = \\ &= \frac{CT}{2}(f(\phi, \theta) + g(\phi, \theta)) \sin \varphi\end{aligned}\quad (5.29)$$

$$\begin{aligned}\widehat{\Delta\phi}_y &= C(f(\phi, \theta) + g(\phi, \theta)) \int_0^T \sin(\omega_{ref}t + \varphi) \sin(\omega_{ref}t) dt = \\ &= C(f(\phi, \theta) + g(\phi, \theta)) \int_0^T -\frac{1}{2}(\cos(2\omega_{ref}t + \varphi) - \cos \varphi) dt = \\ &= \frac{CT}{2}(f(\phi, \theta) + g(\phi, \theta)) \cos \varphi\end{aligned}\quad (5.30)$$

The expressions (5.31) and (5.32) are the change in pitch and yaw respectively for an arbitrary position (ϕ, θ) . The change in pitch and yaw only differs by a factor $\sin \varphi / \cos \varphi$.

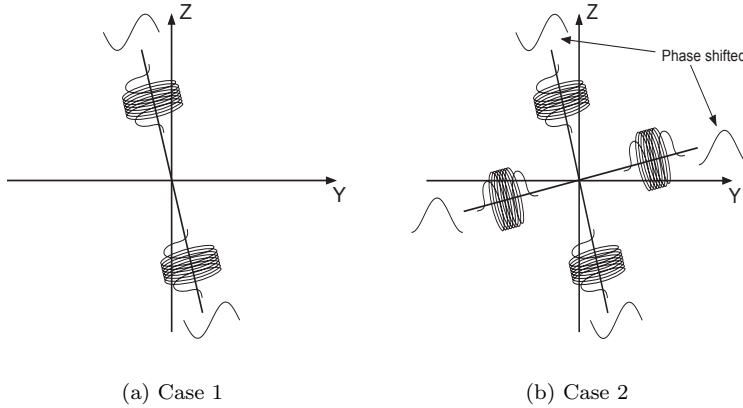


Figure 5.4: Two possible designs for the seeker spin-up system.

Case 2

Now consider a case with two pair of coils placed along two different axes in the yz-plane as shown in Figure 5.4(b). A phase shift φ between the magnetic fields

is introduced since the coils are assumed to act together. Let $\varphi_y = \varphi$ and $\varphi_z = 0$ then (5.23) and (5.24) becomes

$$\begin{aligned}\widehat{\Delta\theta_p} &= C \int_0^T (f(\phi, \theta) \sin(\omega_{ref}t + \varphi) + g(\phi, \theta) \sin(\omega_{ref}t)) \cos(\omega_{ref}t) dt = \\ &= C \int_0^T \frac{1}{2} f(\phi, \theta) (\sin(2\omega_{ref}t + \varphi) + \sin \varphi) + \frac{1}{2} g(\phi, \theta) \sin(2\omega_{ref}t) dt = \\ &= \frac{CT}{2} f(\phi, \theta) \sin \varphi\end{aligned}\quad (5.31)$$

$$\begin{aligned}\widehat{\Delta\phi_y} &= C \int_0^T (f(\phi, \theta) \sin(\omega_{ref}t + \varphi) + g(\phi, \theta) \sin(\omega_{ref}t)) \sin(\omega_{ref}t) dt = \\ &= C \int_0^T -\frac{1}{2} f(\phi, \theta) (\cos(2\omega_{ref}t + \varphi) - \cos \varphi) + \frac{1}{2} g(\phi, \theta) (1 - \cos(2\omega_{ref}t)) dt = \\ &= \frac{CT}{2} (f(\phi, \theta) \cos \varphi + g(\phi, \theta))\end{aligned}\quad (5.32)$$

(5.31) and (5.32) are expanded using (5.26) and (5.27)

$$\widehat{\Delta\theta_p} = \frac{CT}{2} f(\phi, \theta) \sin \varphi = \frac{CT}{2} B_{y0} \sin \phi \sin \theta \sin \varphi \quad (5.33)$$

$$\begin{aligned}\widehat{\Delta\phi_y} &= \frac{CT}{2} (f(\phi, \theta) \cos \varphi + g(\phi, \theta)) = \frac{CT}{2} (B_{y0} \sin \phi \cos \varphi - B_{z0} \cos \phi) \sin \theta = \\ &= \frac{CT}{2} \sqrt{B_{y0}^2 \cos^2 \varphi + B_{z0}^2} \cdot \sin(\phi + \nu) \sin \theta\end{aligned}\quad (5.34)$$

where

$$\nu = \arctan\left(\frac{-B_{z0}}{B_{y0} \cos \varphi}\right)$$

In case 2 there is an additional phase shift of ν in ϕ between $\widehat{\Delta\theta_p}$ and $\widehat{\Delta\phi_y}$. A typical situation would be coil pairs that are located along axes perpendicular to each other. Then a phase shift of $\pi/2$ between the magnetic field is expected. With $\varphi = \pi/2$ the phase shift in ϕ is $\nu = -\pi/2$ since $B_{y0}, B_{z0} > 0$. The phase-shift makes it possible to identify the system as having one pair of coils or two pairs.

The appropriate model must be determined through tests and observations. Direct tests on the real system are difficult for two reasons: The spin coils are embedded in the system and can not be subject to input-output tests. Furthermore, since the gyroscope and the seeker control system is a closed loop system, the effects on the gyroscope caused by the spin coils can not be observed without analyzing the control system. Instead, the effects could be studied using a model. The model was built based on the framework developed in Sections 4.4 and 4.5 and was assumed to

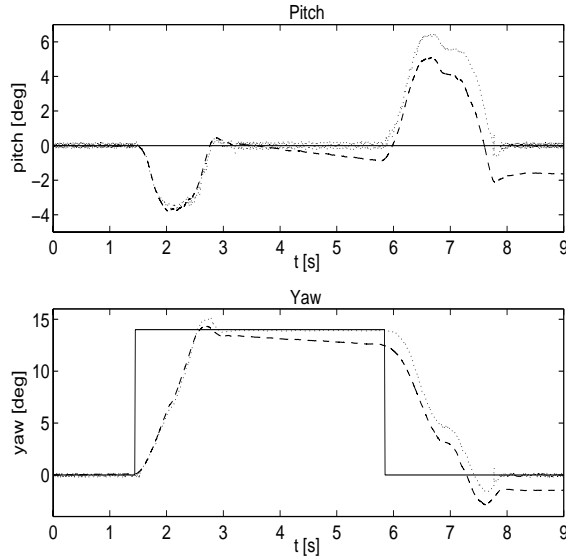


Figure 5.5: Output of model (dashed) and gyroscope (dotted). The solid line is the input signal.

be valid apart from spin coils (the modelling is described in Sections 5.3.2 and 5.4). The control signals for the gyroscope were input to the model. This generated a difference in outputs due to the effects arising from the spin coils. Figure 5.5 shows the pitch and yaw angle of the model and the gyroscope during a test run. The reference signal corresponds to the desired output angles. Viewing the figure it is not unlikely that the model is correct except for the apparent drift.

To relate to the discussion above the drift was plotted for different values of θ and ϕ as shown in Figure 5.6. The control signal that is input to the model corresponds to a fixed gyro at different positions. The plots show that the model (or actually the gyro) is subjected to a torque due to an additional magnetic field. Since the control loop keeps the gyro fixed the effect can not be seen by observing the system.

The drift is given in radians per second for $\phi \in [0, 2\pi]$ and with θ constant. Clearly it is a sinus-like variation that depends on ϕ . The difference in phase between drift in pitch and drift in yaw can be explained by (5.33) and (5.34). However, since (5.33) and (5.34) do not contain a bias term and the plotted drifts clearly show an offset in the amplitude this expression is not adequate to complete the model. The source of the bias is discussed in Section 5.3.2 where also a complement to (5.33) and (5.34) is suggested.

A small phase shift δ can be seen in the plots. This means that the coil-axes are rotated. The rotation is equivalent to a phase shift δ in ϕ . This is compensated for separately in the implementation (see Section 6.1). The spin coils can thus be

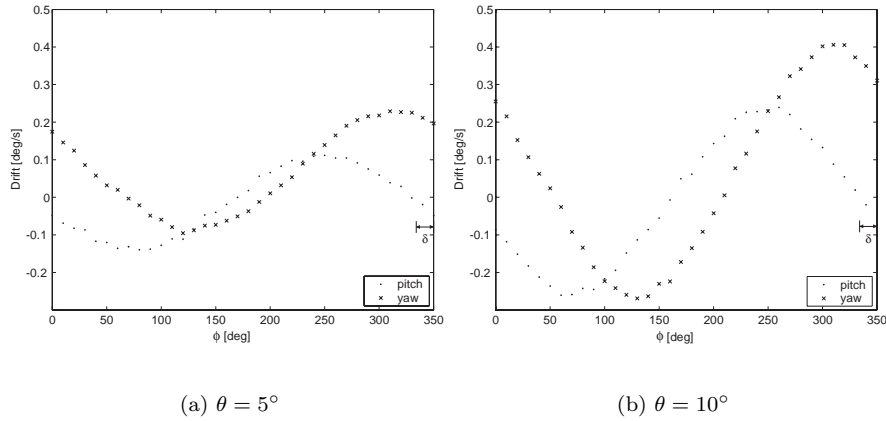


Figure 5.6: Drift in pitch and yaw.

modelled as two pairs of coils generating the magnetic field (case 2)

$$\mathbf{B} = \begin{pmatrix} 0 \\ B_y \\ B_z \end{pmatrix} = \begin{pmatrix} 0 \\ B_{y0} \sin(\omega_{ref}t + \varphi) \\ B_{z0} \sin(\omega_{ref}t) \end{pmatrix} \quad (5.35)$$

This result is worth a comment. The use of two pairs of wire windings is not very surprising. With only one pair (case 1) the system suffers two drawbacks. One is that the magnetic rotor needs a "push" to get started from a stationary position. The second is that the rotor can rotate in either direction. By using a second pair in accordance to case 2 the direction of rotation is determined and no "push" is needed [6].

5.3.2 The Precession Coils

Modelling the precession coils is relatively straightforward when the expression (4.20) in Section 4.5.2 is derived. Often a coil with N number of turns can be approximated with N coinciding single closed loops. Using (4.20) the magnetic field for such a coil is written

$$\mathbf{B}(t) = \frac{\mu_0 N i(t)}{4\pi} \mathbf{\Gamma} \quad (5.36)$$

where

$$\mathbf{\Gamma} = \int_0^{2\pi} \frac{1}{(R^2 + z^2 - 2zR \sin \phi + x^2)^{\frac{3}{2}}} \begin{pmatrix} zR(\sin \phi - R) \\ -xR \cos \phi \\ -xR \sin \phi \end{pmatrix} d\phi \quad (5.37)$$

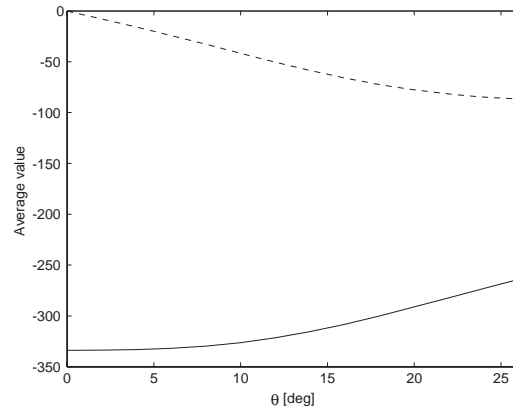


Figure 5.7: Magnetic field integral average value along the x-axis (solid) and y-axis ($\phi = 90^\circ$) (dotted).

The parameters are the radius of the loop R , the radius of the magnet R_m and the number of turns N . The loops of wire are distributed over the width of the coils and a better approximation is gained by repeating the calculation of (5.36). Instead of one loop with N turns, a coil is considered to be made up of M separate loops. The loops have N/M turns and are separated by a distance $d/(M-1)$ along the missile x-axis, where d is the width of the coil. The magnetic fields from the loops are added to give the magnetic field of the coil. The total magnetic field is obtained by adding the contribution from the coils which are separated by a distance D .

In Section 4.5.3 it was shown that the applied torque on the gyroscope could be calculated from the magnetic dipole moment of the magnet and the average applied magnetic field (4.26). It is clear that the average value of the magnetic field will depend on the geometry of the magnet but also the position, or more precisely, the angle measured between the fixed missile x-axis and seeker x-axis, i.e. θ_{sph} . Calculating (5.36) for points in the magnet is time consuming and can not be done during runtime. Instead, since the magnetic field is proportional to the current $i(t)$, a precalculated table is used in the model. The table contains the average of the integral Γ for different values of θ_{sph} . Figure 5.7 shows Γ_x , Γ_{yz} for values of θ_{sph} ranging from 0 to 26. Γ_y and Γ_z are obtained from Γ_{yz}

$$\begin{aligned}\Gamma_y &= \Gamma_{yz} \sin \phi \\ \Gamma_z &= \Gamma_{yz} \cos \phi\end{aligned}$$

Effects from Electromagnetic Induction

As mentioned in Section 3.4 the rotating magnet induces an electromagnetic force in the wire windings in its vicinity. This was the reason why the position of

the magnetic gyro could be determined. Induction also affects the current in the precession coils and thus the resultant magnetic field. The consequence is that the measured signal $i(t)$ in one of the precession coils is the sum of the applied current $i_a(t)$ and the induced current $i_i(t)$.

$$i(t) = i_a(t) + i_i(t)$$

The effect is measurable in the output and induction in the precession coils must be considered in the model. The induced current in the precession coils is equivalent to the current measured in the cage coil due to the similarities in shape and location of the coils (see Section 3.4). This means that the amplitude and phase of the signal are dependent of the orientation of the magnet. Instead of deriving an analytical expression for the current, observations of the model and the system are made.

The test runs (described in Section 5.3.1) indicate that the current gives rise to a slow drift in the output angles. Simulating the model for different positions also proves the fact that the drift is function of the angles θ and ϕ . However, in Section 5.3.1 it was shown that the magnetic field from the spin coils could be modelled as (5.35) and that this described the drift in the gyroscope except for a bias term. By assuming that the bias stems from the induced current a simple model would be a magnetic field that produces this constant drift. Consider the magnetic field

$$B_i = B_0 \sin(\omega_{ref}t + \varphi_i) \quad (5.38)$$

Setting $B_x = B_i$ in (5.23) and (5.24) the change in pitch and yaw due to this magnetic field becomes

$$\begin{aligned} \widehat{\Delta\theta_p} &= C \int_0^T B_0 \sin(\omega_{ref}t + \varphi_i) \cos(\omega_{ref}t) dt = \\ &= CB_0 \int_0^T \frac{1}{2} (\sin(2\omega_{ref}t + \varphi_i) + \sin \varphi_i) dt = \\ &= \frac{CTB_0}{2} \sin \varphi_i \end{aligned} \quad (5.39)$$

$$\begin{aligned} \widehat{\Delta\phi_y} &= C \int_0^T B_0 \sin(\omega_{ref}t + \varphi_i) \sin(\omega_{ref}t) dt = \\ &= CB_0 \int_0^T -\frac{1}{2} (\cos(2\omega_{ref}t + \varphi_i) - \cos \varphi_i) dt = \\ &= \frac{CTB_0}{2} \cos \varphi_i \end{aligned} \quad (5.40)$$

This means that the drift will be independent of the position of the gyroscope. The relative drift between the angles is determined by φ_i according to

$$\frac{\widehat{\Delta\theta_p}}{\widehat{\Delta\phi_y}} = \frac{\sin \varphi_i}{\cos \varphi_i} \quad (5.41)$$

Parameter	Description
N	Number of turns in the precession coils
R	Radius of the precession coils
R_m	Radius of the magnet
$\mathbf{I} (I, I_0)$	Moments of inertia of the gyroscope
m	Magnetic dipole moment (magnitude)
p_x	Spin-rate of the gyroscope, i.e. angular velocity along the seeker x-axis
B_{0y}, B_{0z}	Amplitudes of the magnetic fields generated by the spin coils
φ	Phase between the magnetic fields generated by the spin coils
δ	Phase shift in ϕ due to placement of spin coils
B_0	Amplitude of the magnetic field resulting from the induced current
φ_i	Phase of the magnetic field resulting from the induced current

Table 5.1: Parameters in the model.

5.4 Parameter Estimation

To be able to implement and validate the model the unknown parameters must be estimated or guessed. This is normally done through experiments on the real system. Table 5.1 is a summary over parameters in the gyro model. In view of (5.9), (5.16), (5.18) and (5.36) the output of the model, i.e. the angles yaw and pitch, is directly proportional to the parameters N , m and inversely proportional to I and p_x . These parameters can thus be collected in one parameter K

$$K = \frac{Nm}{Ip_x} \quad (5.42)$$

This property of the system simplifies parameter estimation considerable. First of all, instead of estimating four parameters one single parameter can be estimated. Furthermore, since K is proportional to the output estimation is a simple matter of comparing model and system step-response. However, parameters p_x and \mathbf{I} are used in the modelling process (see Section 5.1) and must be estimated separately. The spin-rate p_x is approximated from the measured values of ω_{ref} (see Section 5.1).

The mass of the gyroscope is assumed to be concentrated to the outer rim of the rotor, and an appropriate value of the elements in \mathbf{I} can be found by treating the gyro as a cylindrical shell [11]. In the final implementation of the model rough estimations of the parameters are used instead of K to clarify the correspondence to the real system.

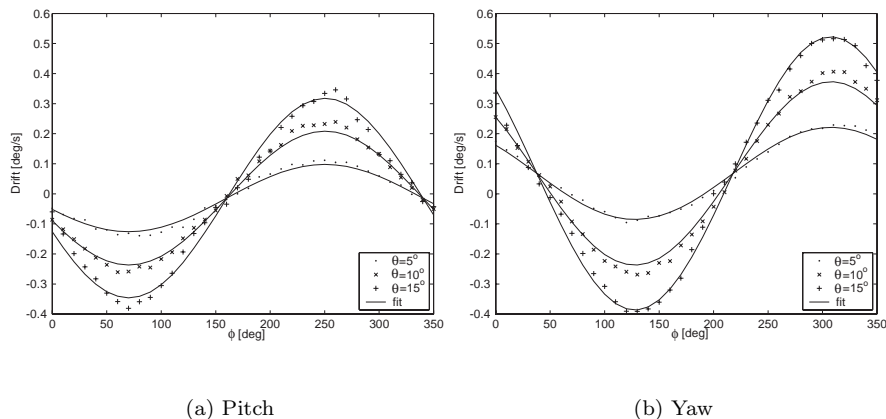


Figure 5.8: (5.43) fitted to observations of drift in pitch ($\Delta\theta_p$) and yaw ($\Delta\phi_y$).

The unknown parameters of (5.35) and (5.38); B_{y0} , B_{z0} , φ , δ , and B_0 , φ_i respectively can be estimated through observations of the system. The magnetic field from the spin coils can not be measured, instead the data consists of observations of model output from the test runs that was described in Section 5.3.2. The parameters are thus determined by fitting (5.33) and (5.34) to data. The data also contain a constant term that determines the parameters of (5.38) (see Section 5.3.2) and thus by adding a constant to (5.33) and (5.34) B_0 and φ_i can be estimated. These functions are non-linear and the parameters are estimated using non-linear regression, e.g. the Gauss-Newton method. The least square non-linear regression model is

$$y_t = f(\beta, \mathbf{x}_t) + \epsilon_t \quad (t = 1, \dots, n)$$

$$\min_{\beta} S(\theta) = \sum_{t=1}^n (y_t - f(\beta, \mathbf{x}_t))^2$$

where the matrix \mathbf{x}_t is the independent variable and y_t is a vector of observations. ϵ_t is a vector of random disturbances ($E\{\epsilon_t\} = 0$) and β is the parameters to be estimated. The function f is given by (5.33) or (5.34)

$$f(\beta, \mathbf{x}_t) = \beta_1 \sin(x_{t1} + \beta_2) \sin x_{t2} + \beta_3 \quad (5.43)$$

Since (5.33) and (5.34) are identical, except for the parameters, one function is adequate. The term β_3 represents (5.39) and (5.40). y_t are observations of $\Delta\theta_p$ or $\Delta\phi_y$ generating two solutions and two sets of parameters β . Identification of the

parameters using (5.33), (5.34), (5.39) and (5.40) yields

$$\begin{aligned}\beta_1 &= \frac{CT}{2} B_{y0} \sin \varphi \\ \beta'_1 &= \frac{CT}{2} \sqrt{B_{y0}^2 \cos^2 \varphi + B_{z0}^2} \\ \beta_3 &= \frac{CT}{2} B_0 \sin \varphi_i \\ \beta'_3 &= \frac{CT}{2} B_0 \cos \varphi_i \\ \delta &= \beta_2 \\ \nu &= \beta'_2 - \beta_2\end{aligned}\tag{5.44}$$

The primed parameters are used to separate the two solutions. Knowing C and T the desired parameters can be determined from (5.44). The fitted functions are plotted in Figure 5.8.

Chapter 6

Implementation and Validation

This chapter describes the realization of the mathematical model. The implementation in software is described and the results from various simulations are presented.

6.1 Implementation

The model was implemented in Simulink[®], which is an extension of MATLAB[®] for modelling, simulation and analysis of dynamic systems. In Simulink[®] a graphical user interface is used for building models as hierarchical block diagrams. The system can be viewed at top level or in greater detail by viewing the blocks inside the higher level blocks.

The Simulink[®] model is a stand-alone model and can only be used off-line in the MATLAB[®] environment. For use in the real-time application the model had to be implemented in C-code. This was done using RTW (Real-Time Workshop[®]) in Simulink[®]. With RTW portable and customizable C-code can be generated from Simulink[®] models to create implementations of the models suitable for real-time operation [7]. It also provides a framework for running generated code in real-time, tuning parameters, and viewing real-time data, but these features was not used.

6.1.1 Simulink[®]

The complete model implemented in Simulink[®] is shown in Figure 6.1. This is the top level description where different parts of the model are divided into subsystems. As was concluded in Section 5.3 the seeker is affected by the spin coils when running in the HWIL environment, but during actual flight the seeker is not. To be able to use the model in both cases a signal `Spin Coils On/Off` is added. The effects from induction is also made optional. The blocks `DataInput` and `DataOutput` are the

model I/O-structures implemented as so called S-functions [8]. These are further described in Section 6.1.2. Here follows a description of the subsystems included in the model. It should be noted that before generating the real-time code some minor modifications were made to this Simulink[®] model in order to optimize the code slightly. However, the function is still the same. Subsystems not described here can be found in Appendix A.

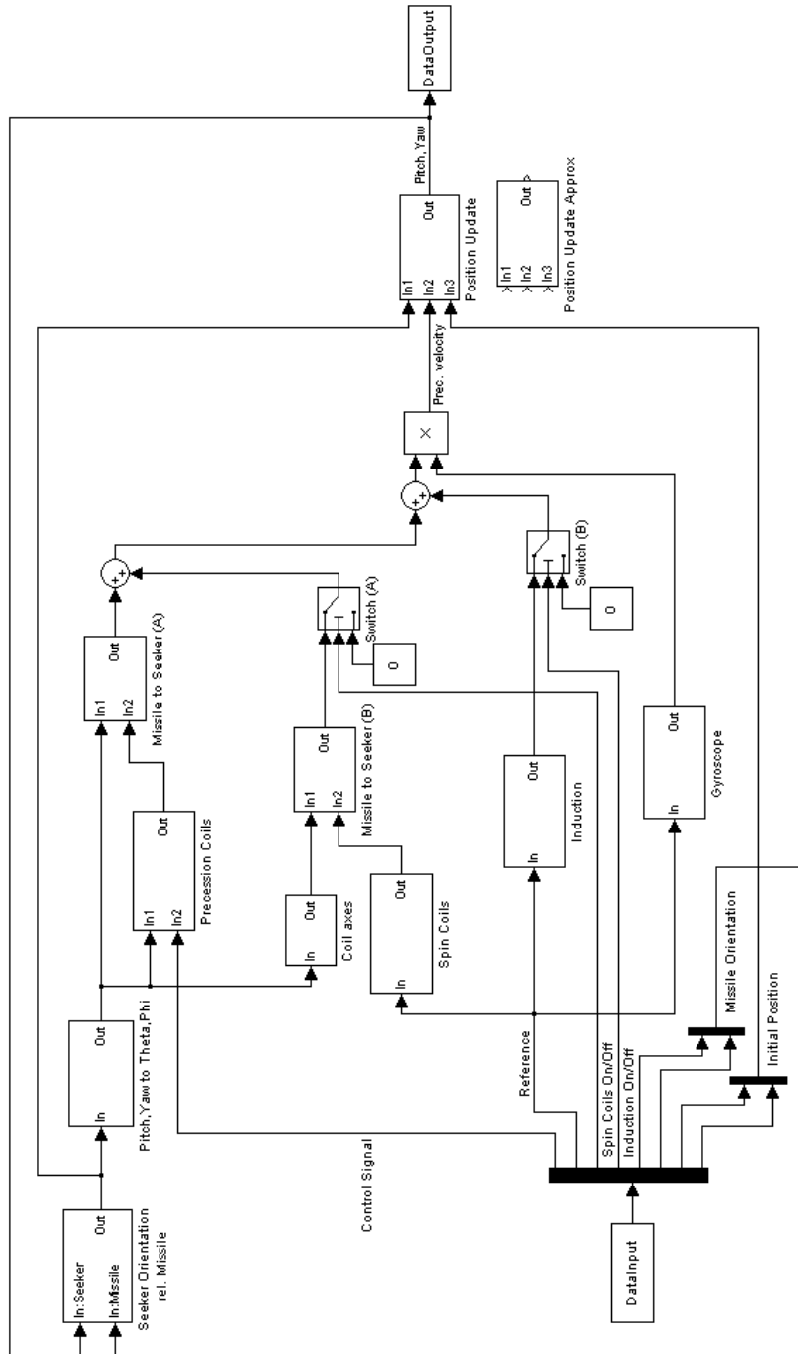


Figure 6.1: The model implemented in Simulink®.

Precession Coils

Input Signal 1: Seeker orientation in spherical angles ϕ and θ

Input Signal 2: Control signal $i(t)$

Output Signal: Magnetic field acting on the gyroscope relative to the missile

The blocks `Integral_x` and `Integral_yz` are look-up tables containing the average magnetic field described in Section 5.3.2. The values are also plotted in Figure 5.7. The trigonometric function blocks are used to get the magnetic field in the y- and z-coordinate from `Integral_yz`. Block `K1` is a constant that converts a control signal voltage to the corresponding current, i.e. $K1 = 1/R$ where R is the resistance of the coil. The factor `K2` is given by

$$K2 = \frac{\mu_0 N}{4\pi}$$

where N is the number of turns in the coils and μ_0 is the permeability of free space. The precession coils subsystem is shown in Figure 6.2.

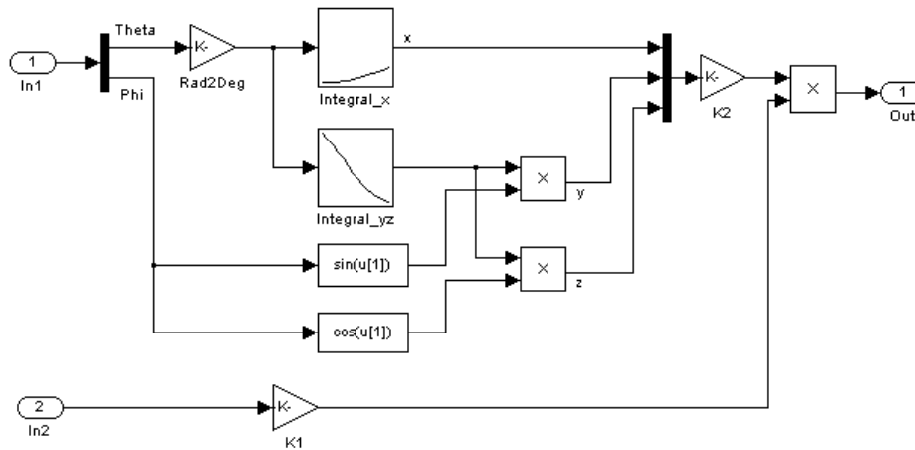


Figure 6.2: Precession Coils subsystem

Missile to Seeker

Input Signal 1: Seeker orientation relative to the missile in spherical angles ϕ and θ

Input Signal 2: Magnetic field acting on the gyroscope relative the missile

Output Signal: Magnetic field in the x-direction acting on the gyroscope relative to the seeker

The trigonometric function blocks contains the transformation vector \mathbf{d}_{xIS} given by (4.3) in Section 4.3.2. The result from the multiplication is summarized to give

B_{xS} in (5.8), see Section 5.1.1. Missile to Seeker (A) is equivalent to Missile to Seeker (B). The subsystem is shown in Figure 6.3.

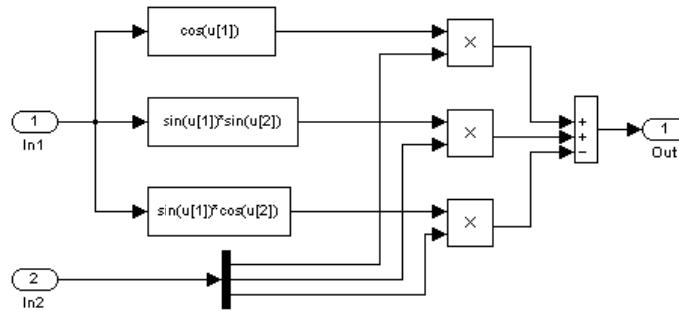


Figure 6.3: Missile to Seeker subsystem.

Spin Coils

Input Signal: Gyroscope spin-angle reference

Output Signal: Magnetic field acting on the gyroscope relative to the missile

Blocks B_y and B_z contain the modelled magnetic field expressed as (5.35), where the numerical values are the estimations of B_{y0} and B_{z0} . The phase shift in (5.34) is implemented as a separate block (phase). Block $K3$ contains a factor that depends on the time interval in which the drift was measured, e.g. T in (5.33) and (5.34). The spin coils subsystem is shown in Figure 6.4.

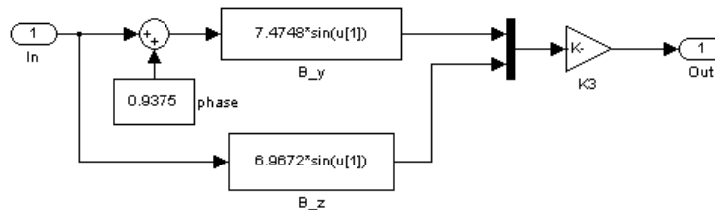


Figure 6.4: Spin Coils subsystem.

Induction

Input Signal: Gyroscope spin-angle reference

Output Signal: Magnetic field acting on the gyroscope relative to the missile

Implementation of (5.38) with estimated values of B_0 and φ_i . Block K4 is analogous to K3 in block Spin Coils. The induction subsystem is shown in Figure 6.5.

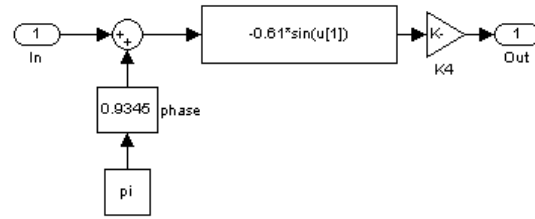


Figure 6.5: Induction subsystem.

Pitch,Yaw to Theta,Phi

Input Signal: Seeker orientation relative to the missile in angles pitch and yaw
 Output Signal: Seeker orientation relative to the missile in spherical angles ϕ and θ

The function blocks implement the transformation given by (4.6). The function `atan2` is a four quadrant inverse tangent which gives angles in the interval $[-180, 180]$. ϕ is defined for $[0, 360]$ and this can be achieved by unwrapping if yaw < 0 . The subsystem is shown in Figure 6.6.

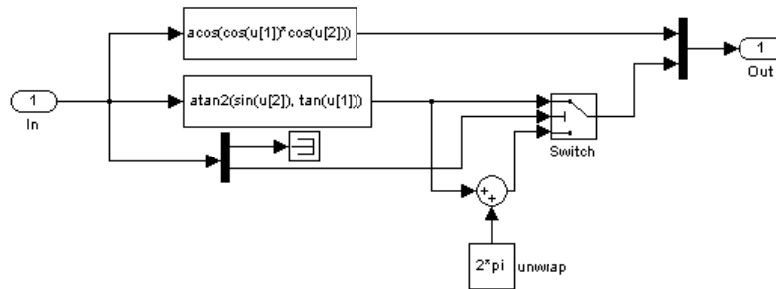


Figure 6.6: Pitch,Yaw to Theta,Phi subsystem.

Gyroscope

Input Signal: Gyroscope spin-angle reference
 Output Signal: Gyroscope information

Blocks `m_y` and `m_z` implements the rotating magnetic dipole vector \mathbf{m} stated in (5.10), with an estimated value of m . The phase is used to adjust the implemented vector to the reference. Block `K5` is the factor containing the constant spin velocity p_x and the moment of inertia I along the x-axis according to

$$K5 = \frac{1}{Ip_x}$$

The gyroscope subsystem is shown in Figure 6.7.

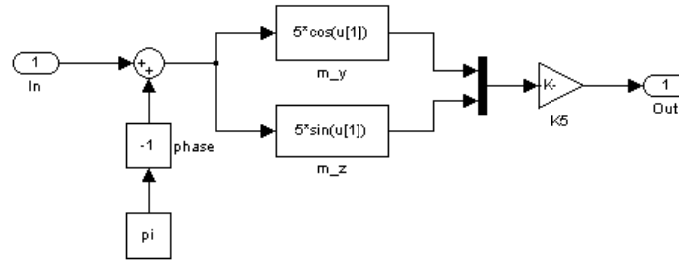


Figure 6.7: Gyroscope subsystem.

Position Update / Position Update approx.

- Input Signal 1: Seeker orientation relative to the missile in angles pitch and yaw
- Input Signal 2: Precession velocity relative to the seeker
- Input Signal 3: Initial position of seeker in pitch and yaw
- Output Signal: Updated seeker orientation in angles pitch and yaw

Block `C_SI`: x,y,z transforms a position given in pitch and yaw to the corresponding Cartesian coordinate in the inertial frame (see Appendix A.3, A.4). $\dot{x}(t)$ (`x_dot`) is calculated using (5.18) in Section 5.2. The updated output in angles yaw and pitch are the output y_1 and y_2 respectively in (5.18). The position update subsystem is shown in Figure 6.8.

The **Position Update Approx** block simply contains an integration of the input precession velocity.

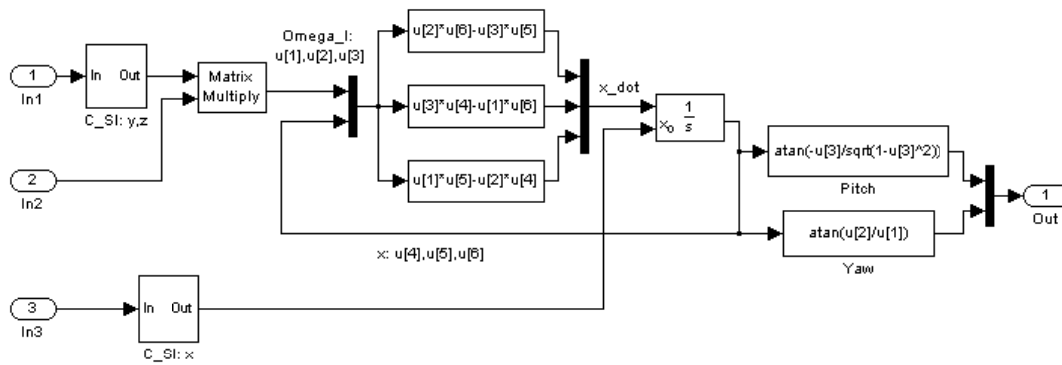


Figure 6.8: Position Update subsystem.

6.1.2 Real-Time Workshop[®]

For a specific application suitable code must be generated, and to specify how this is done Real-Time Workshop[®] provides different code formats. The target system on which the final real-time application is executed is a PC with a real-time operating system (see Section 2.3). This defines which code format to use. With no restrictions on code size or memory usage a generic real-time target code format was used. It is the most comprehensive code format and it supports almost all blocks included in the Simulink[®] package. The generic real-time target also supports nonreal-time simulations which is useful as a starting point to create a real-time model prototype that does not use real-time operating system tasking primitives. This feature was used to validate the generated code before it was incorporated with the larger system. The procedure involved building an executable program with the model as a stand-alone application. It will however not be described any further in this thesis.

The generic code generated by RTW could be customized by modifying certain script files called Target Language Compiler files. This served as a way to optimize or otherwise control the overall code generation. Incorporating the model into the main application involved primarily two things; writing or customizing supporting code to interface the generated model code and creating a model I/O-structure.

Interfacing the Generated Code

Exported entry points make it possible to interface hand-written code to the generated code. Entry points are functions that include code to allocate memory, initialize the model states, update block output, and to update continuous and discrete states. See Appendix B for a description of model functions that are of interest for the run-time interface. The interface consists of model configuration

code and most importantly, the code that calls the generated functions. Besides the initialization and termination of the model which is done only once when the application starts and terminates respectively, the most central function is to execute the model and store the output. This is carried out in the following manner

- Model input data is presented
- A routine performing one step of the model is called
- Model output data is retrieved

The one step routine in turn handles calls to the model functions. The model output function first calls all the blocks in the model and have them produce their output. The update function then calls the integrator block and have it update its continuous states. Input and output data are contained in arrays that are passed as arguments to the function that executes the model. This procedure represents an execution loop and has to be carried out for each sample. Model execution is illustrated by the flow chart in Figure 6.9.

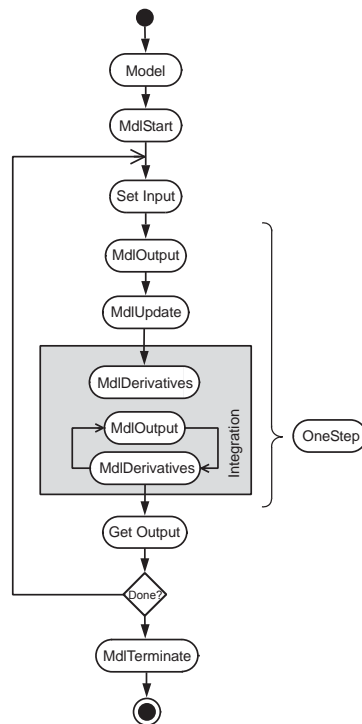


Figure 6.9: Flow chart describing the execution of the model in the simulator. The function **Model** and functions with prefix **Mdl** are the exported entry points generated by RTW (see Appendix B).

The Model I/O-structure

For a model to be able to receive input data and deliver output data it needs certain functions to handle communication. In the Simulink® model these functions are represented by an input block and an output block. This is an analogy to when device drivers are used by an application to communicate with hardware such as I/O boards. In this particular application the actual hardware interface is implemented elsewhere in the main application code while the blocks in the model solely manages data transfer between the model and the main program.

The I/O blocks are constructed using S-functions. An S-function is a computer language description of a Simulink® block that is defined by code written by the user. I/O blocks are implemented using the C MEX S-function format, see [8]. The I/O blocks in the model use a special data structure to store values. This data structure can be accessed by the application interface to set input values in the input block and get output values from the output block.

6.2 Validation

Validation of the model was done by comparing simulated output with the output from the real system. The gyroscope is controlled by a control unit (regulator) in a closed loop structure and simulations are done by feeding identical control signals to the model. The input is the desired output angles (pitch, yaw) or $(\theta_{sph}, \phi_{sph})$ and the target roll rate.

The output of the model is the position of the gyroscope given in angles pitch and yaw relative to the inertial frame. However, no similar output signals exist for the real system. Instead the position of the gyroscope must be estimated from the cage signal. This estimation is based on empirical observations of amplitude and phase of the cage signal and corresponding measured angles of the gyroscope. Due to the nature of the cage signal the accuracy lessens for small angles. This clearly limits the possibility to validate the model properly since the output to which the simulated output is compared is dependent on the quality of the estimation.

6.2.1 Step-Response and Target Tracking

The performed simulations are divided into step-response and target tracking. The step-response tests are suitable when comparing maximum tracking velocity of the model and the gyro. This follows from the assumption that the gyroscope is accelerated to its maximum precession velocity during a step. Furthermore, the maximum tracking velocity is expected to vary with the position of the gyro since the torque depends the direction of the magnet relative the coils (this is concluded in Section 5.1.1). Steps are therefore applied for different initial positions. Target tracking simulations are closer to the actual operation of the seeker and the gyro system. These simulations will show a more general behavior of the model for different tracking velocities and over a broader range of positions.

Step-Response Simulations

The step-responses of the model and the gyroscope are plotted in Figures 6.10 and 6.11. Here the pitch angle is kept constant at zero while the initial value of yaw is varied. The input step is a desired yaw angle. The amplitude of the steps is 2.5 degrees and the initial position ranges from 0 to 7.5 degrees. From these simulations the variations in maximum tracking velocity can be analyzed and compared. In addition to the small steps a large step where the gyroscope is taken from 0 degrees to 10 degrees. The outputs are shown in Figures 6.12 and 6.13.

Target Tracking Simulations

Figures 6.14 - 6.16 show the outputs of three target tracking simulations. In the first scenario the target appears in the seeker FOV positioned 3.6 degrees offset from the seeker LOS. The seeker turns towards the target at maximum rate and starts tracking it. As the target moves away from the seeker it begins a rolling motion at a constant angular velocity of 7 degrees per second.

The second scenario is similar to the first scenario only this time the target appears at a 6.4 degree offset from the LOS and the angular velocity during the roll is near the maximum tracking velocity of the seeker.

In the third scenario the seeker tracks the target from the start of the simulation. Initially the target is moving away from the seeker along the x-axis. At time $t = 1.8$ seconds the target makes a slow turn in the positive y direction to an angle near the maximum turning angle of the seeker. At time $t = 7$ seconds it starts to roll at about 6 degrees per second.

6.2.2 Comments on the Plots

At first sight the model seems to have problems reproducing the step-responses of the gyroscope. In this case the response in yaw is the most interesting to look at. The plots in Figure 6.10(a) show that the model is slower than the gyroscope in the range 0-2.5 degrees while the situation is the opposite in the range 2.5-5 degrees as shown in Figure 6.10(b). However, the accuracy of the position estimates during this test run is considered to be less than 0.4 degrees. In Figures 6.10(a) and 6.11(a) for example, the apparent outliers at time $t = 1.25$ seconds are indications of poor estimation. Also, an interesting comparison can be made between the results from the large step in Figure 6.12 and the smaller step-responses in Figure 6.10. Figure 6.12 shows that the model simulates the interval 0 to 2.5 degrees fairly well as opposed to what is seen in Figure 6.10(a). From Figures 6.10(b), 6.10(c), 6.10(d) and 6.12 it is seen that the velocity of the gyroscope starts to decrease around 3.5 degrees and then again increase after the gyroscope reaches 6 degrees. The tracking velocity is actually peaking around 9 degrees in view of Figures 6.10(d) and 6.12. This is unexpected since the torque acting on the gyroscope should decrease with an increasing angle (see Section 4.5.3). It is difficult to conclude if the varying velocity and the difference between model and gyroscope output seen in plots stems from properties not modelled or problems estimating the position. The simulated pitch angle shows no dramatic deviations from the estimated output. The most obvious difference that can be commented is the offset that appears after the change (seen as a dip) during the step. No corresponding offset is seen in the output of the gyroscope. Still, the offset is smaller than 0.2 degrees for the steps in Figure 6.10 and 6.11 can be considered within an adequate confidence interval. The outputs from the target tracking scenarios are plotted in Figures 6.14, 6.15, 6.16. Simulations of tracking below the maximum velocity (Scenario 1, Figure 6.14) and simulations of tracking near the maximum velocity (Scenario 2, Figure 6.15) show good results. The slight difference in velocity can be seen in the amplitude of the pitch and yaw angle. In Scenario 3 the seeker is tracking a target in a wide angle and here the model has more difficulties to simulate the motion. The output is plotted in Figure 6.16. The simulated pitch rate is too slow while the yaw rate is faster than the yaw rate of the gyroscope. This non-symmetry might be the effect of inadequate modelling of the magnetic field generated by the spin coils. In Section 5.3.1 the magnetic field was assumed to be uniform over the magnet which is a good approximation for small angles. In accordance the parameters in (5.35) and (5.38)

was estimated using observations where the angle was smaller than 11 degrees. Another observation is that the simulated yaw angle differs almost exclusively in its negative half plane. The most obvious explanation is that the gyroscope is not symmetric while the model is (and thus inadequate). However, there are no signs of this non-symmetry in the other simulations so again it might be interpreted as badly estimated gyro positions.

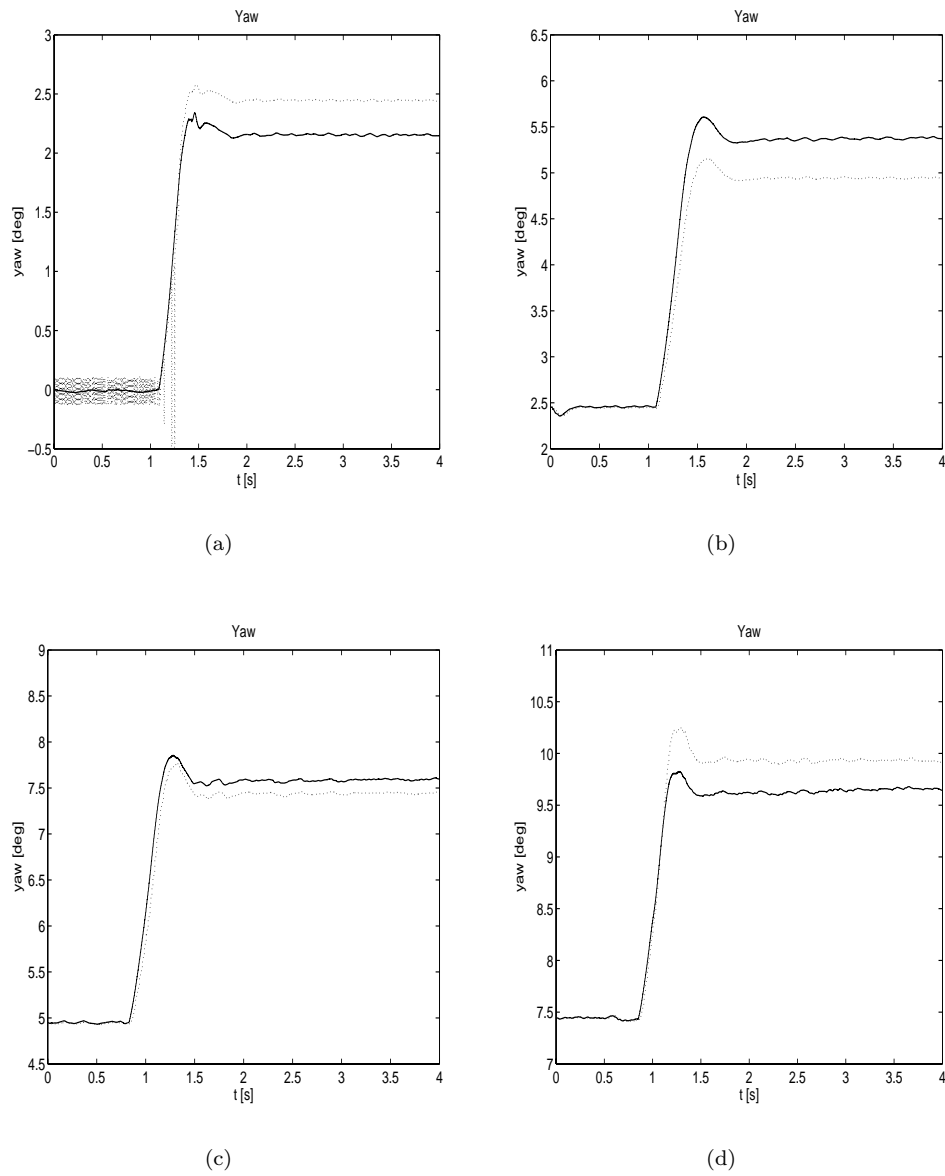


Figure 6.10: Step-responses (yaw) for different initial positions. The input step is 2.5 degrees in yaw. Solid lines are the simulated position (model output) and dotted lines are the estimated position of the gyroscope.

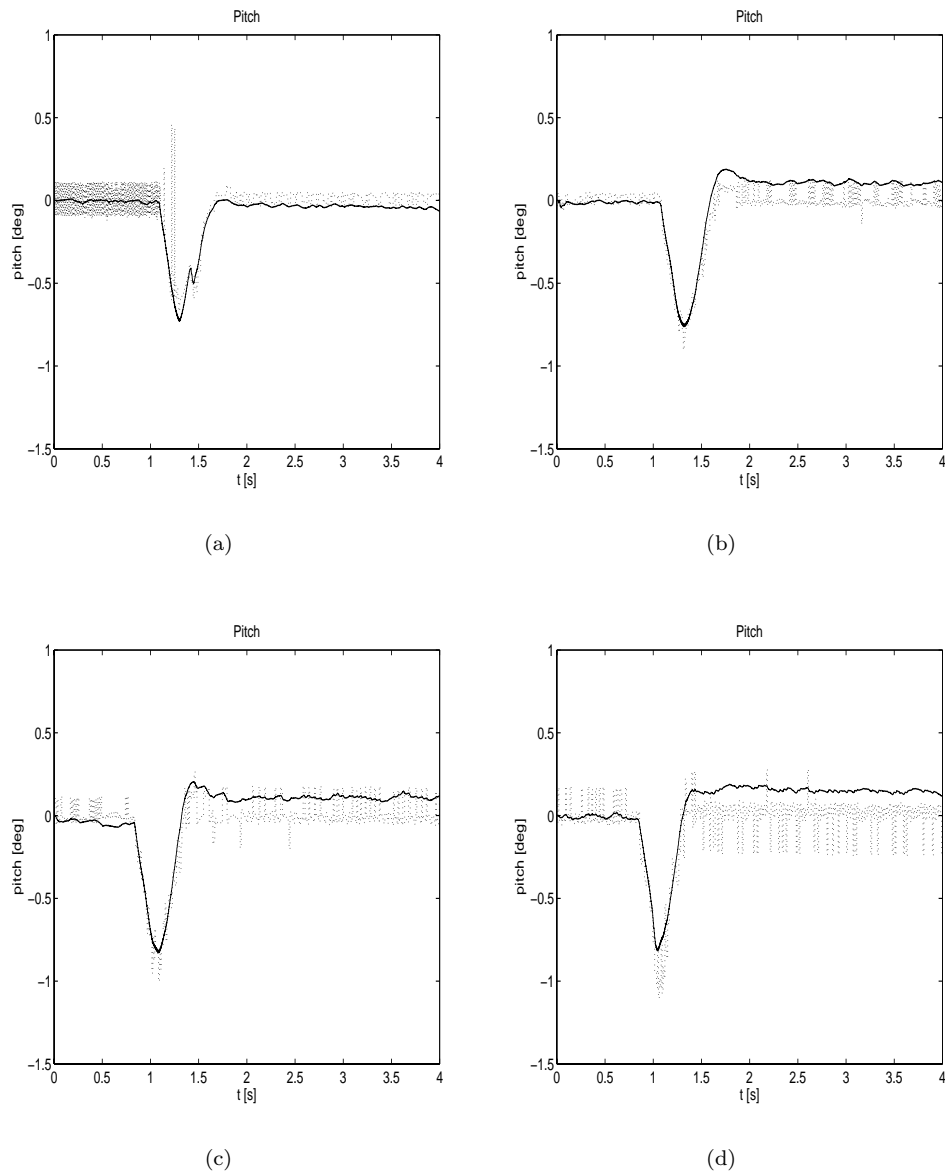


Figure 6.11: Step-responses (pitch) for different initial positions. The input step is 2.5 degrees in yaw. Solid lines are the simulated position (model output) and dotted lines are the estimated position of the gyroscope.

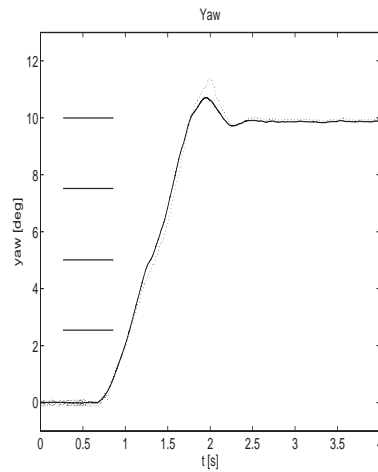


Figure 6.12: Step-response (yaw) for a input step of 10 degrees in yaw (initial position $\theta_p = \phi_y = 0$). Solid lines are the simulated position (model output) and dotted lines are the estimated position of the gyroscope. The intervals indicated by lines correspond to the smaller steps in Figure 6.10.

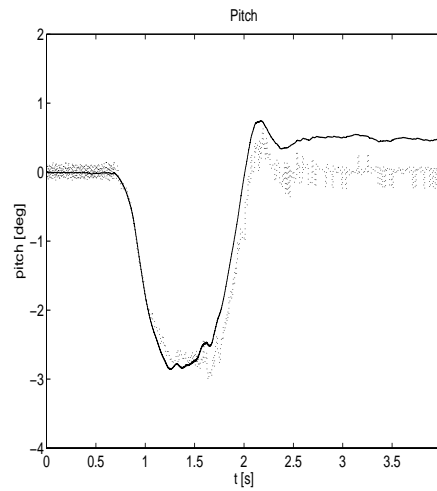


Figure 6.13: Step-response (pitch) for a input step of 10 degrees in yaw (initial position $\theta_p = \phi_y = 0$). Solid lines are the simulated position (model output) and dotted lines are the estimated position of the gyroscope.

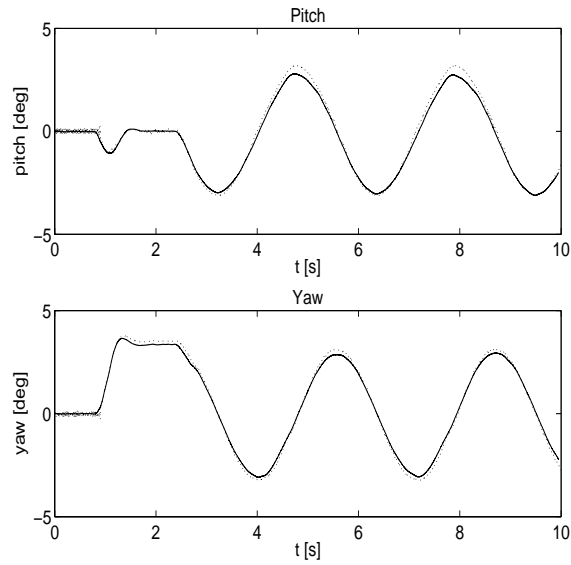


Figure 6.14: Scenario 1 target tracking simulation output. Solid lines are the simulated position (model output) and dotted lines are the estimated position of the gyroscope.

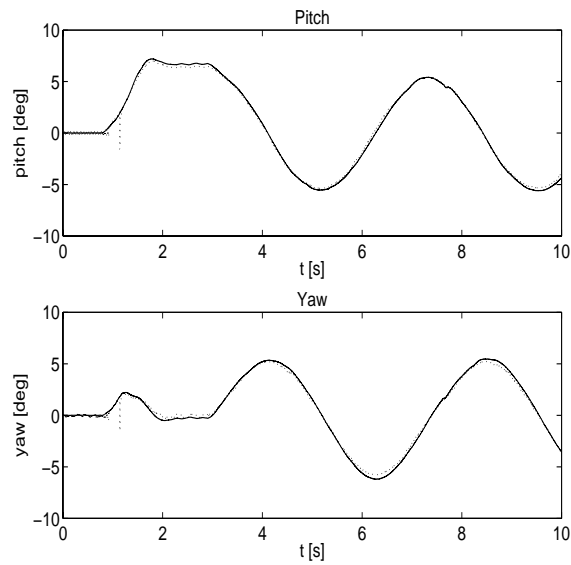


Figure 6.15: Scenario 2 target tracking simulation output. Solid lines are the simulated position (model output) and dotted lines are the estimated position of the gyroscope.

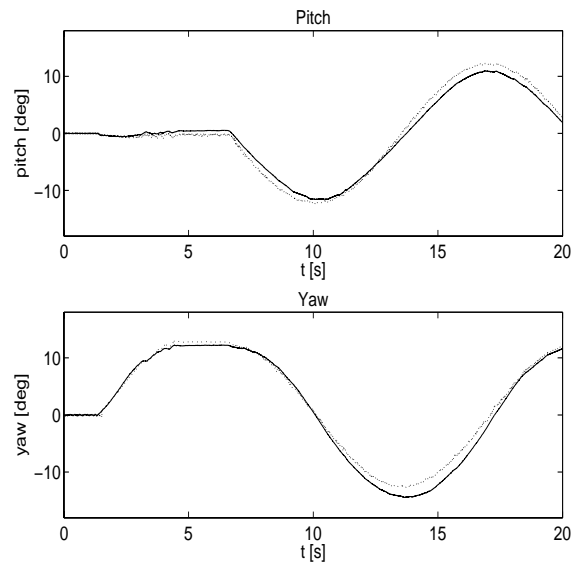


Figure 6.16: Scenario 3 target tracking simulation output. Solid lines are the simulated position (model output) and dotted lines are the estimated position of the gyroscope.

Chapter 7

Conclusions

In this thesis a real-time model of the seeker gyroscope in a MANPAD IR guided missile has been developed and tested. The thesis also describes an appropriate methodology for modelling and model integration with consideration to a HWIL environment. The result is a gyro model module that is able to simulate the real system fairly well yet fast enough to satisfy the real-time demands. The model can be used in the simulator as intended.

In the methodology developed, the model is built as a stand-alone non-real-time application in Simulink[®] separate from the other blocks in the simulator environment. The model is then easily optimized and suited for real-time operation using Real-Time Workshop[®] (RTW). The generic C-code generated by RTW can eventually be integrated into the main application in a rather straight forward manner.

The chosen method and use of Simulink[®] as the development environment has some advantages. The modelling procedure can be carried out independently and without consideration to the main application. This allows for early non-real-time testing and analysis of simulations. With Simulink[®] this is done efficiently in MATLAB[®]. Furthermore, RTW enables testing of the real-time model as a stand-alone application by generating executable code. In that way the model does not have to be integrated into the real-time simulator just to test speed and other real-time criterions. The model can be executed on a workstation not running MATLAB[®].

The gyro model was built mainly using the system description in that the physical mechanisms of the subsystems were represented by known equations and relations. Since such a model often suffers from higher computational complexity than its black-box equivalent the choice is not obvious. However, the model could be tuned for use in the limited range of rotation applicable to the system (see Section 3.3) and in that way its complexity could be kept sufficiently low. The key approximations include the motion of the gyroscope as steady state precession and the integration of angular velocity about the x- and y-axes to get the position of the gyroscope. The most apparent weakness of the model is operation in wide

angles, i.e. when the gyroscope is rotated to position near its outer limit.

7.1 Future Work

The intended extension of the work described in this thesis is to build analogous models of similar systems. Although these systems might be more advanced the methods and most of the model framework will be useful. However, at some points the model can be further developed and this thesis is concluded with a few propositions to future work.

In this thesis approximations are almost exclusively based on empirical studies. Since no thorough investigation of how the output of the model depends on a certain approximation has been done the possibility to improve the performance is somewhat limited. A better understanding of the weaknesses of the current model could therefore be attained by analyzing the effect of the approximations. This would involve deriving mathematical expressions for the errors or at least finding good error estimations.

A more extensive and, to some extent, a less approximative model is possible if the simulation speed is improved. This is achieved by tuning the performance of the block diagram and the generated code. Examples include tabulating trigonometric functions and using embedded S-function C-code in the generated code (in the current implementation the S-function is invoked by calls to the S-function API (Application Program Interface) routines). Optimization techniques are discussed in [7].

It should be noted that to be able to make a complete study of the performance of the model the position estimation of the gyroscope needs to be more accurate. This problem was mentioned in Section 6.2.2. Since the output of the gyro model is considered to be within an adequate confidence interval any suggested improvement would be hard to validate. An important and necessary task is hence to refine the position estimation.

Bibliography

- [1] D.K. Cheng. *Field and Wave Electromagnetics*. Series in Electrical Engineering. Addison-Wesley, N.Y. USA, 2nd edition, 1989.
- [2] J.H. Ginsberg. *Advanced Engineering Dynamics*. Cambridge, 40 West 20th Street, N.Y. USA, 2nd edition, 1995.
- [3] T. Glad and L. Ljung. *Modellbygge och simulering*. Studentlitteratur, Lund, Sweden, 1991. In Swedish.
- [4] J. Safko H. Goldstein, C. Poole. *Classical Mechanics*. Addison-Wesley, 1301 Sansome St., San Francisco, USA, 3rd edition, 2002.
- [5] P. Hackman. Krypa-gå. Linköping, Sweden, 1997. In Swedish.
- [6] Internet. *All About Circuits*. http://www.allaboutcircuits.com/vol_2, (Acc. 2003-12-02).
- [7] The MathWorks, Inc., 3 Apple Hill Drive, Natick, MA. USA. *Real-Time Workshop: For Use with Simulink – User’s Guide*, 2002. Version 5.
- [8] The MathWorks, Inc., 3 Apple Hill Drive, Natick, MA. USA. *Simulink: Model-Based and System-Based Design – Writing S-Functions*, 2003. Version 5.
- [9] J.L. Meriam and L.G. Kraige. *Engineering Mechanics: Dynamics*, volume 2. Wiley, N.Y. USA, 4th edition, 1998.
- [10] H. Nichols. *Modelling of Dynamical Systems*, volume 1 of *IEE Ccontrol Engineering Series*. Peter Peregrinus Ltd, Stevenage, UK, 1980.
- [11] C. Nordling and J. Österman. *Physics Handbook*. Studentlitteratur, Lund, Sweden, 5th edition, 1996.
- [12] R. Pettersson. Modell av IR-målsökare med tungt gyro. Technical Report FOA-R-98-00805-616-SE, Division of Command and Control, FOI, Linköping, Sweden, 1998.
- [13] A. Pytel and J. Kiusalaas. *Engineering Mechanics: Statics and Dynamics*. Harper-Collins, 10 East 53rd Street, N.Y. USA, 1996.

- [14] L. Tydén and M. Bergvall. Slutrapportering projekt HÄLGE år 2002. 02-H491, November 2002.
- [15] W.L. Wolfe and G.J Zissis. *The Infrared Handbook*. IRIA Series in Infrared and Electro-Optics. ERIM, Ann Arbor, MI, USA, revised edition, 1993.

Appendix A

Supplementary Subsystems of the Model

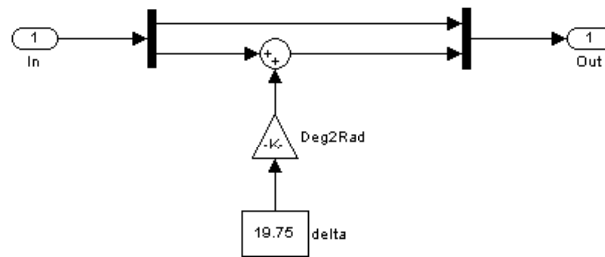


Figure A.1: Coil Axes subsystem.

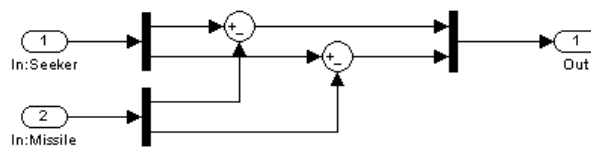


Figure A.2: Seeker Attitude rel. Missile subsystem.

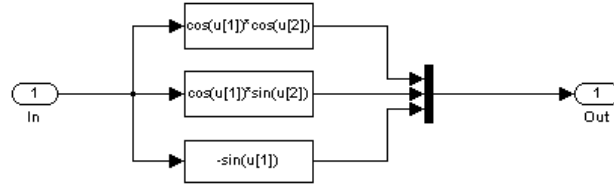


Figure A.3: C_Sl:x subsystem.

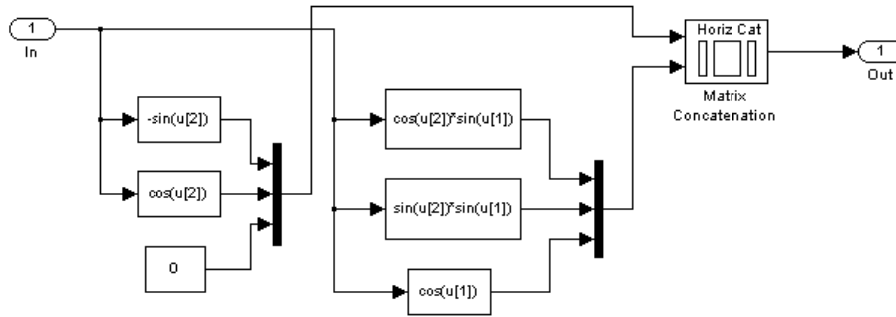


Figure A.4: C_Sl:y,z subsystem.

Appendix B

Functions Generated by Real-Time Workshop[®]

Function	Description
Model()	Model registration function. This function initializes the work areas (e.g. allocating and setting pointers to various data structures) needed by the model.
MdlStart()	The run-time interface starts execution by calling MdlStart. This routine is called once at startup. MdlStart includes code for initialize states for each block in the root model that has states, code generated by the one-time initialization function for each block and code for each block that has a constant sample time.
MdlOutputs()	Updates the output of blocks at appropriate times. This routine is invoked by the run-time interface during major and minor time steps. The major time steps are when the run-time interface is taking an actual time step (i.e. it is time to execute a specific task). If the model contains continuous states, the minor time steps will be taken. The minor time steps are when the solver is generating integration stages, which are the points between major outputs. These integration stages are used to compute the derivatives used in advancing the continuous states.
MdlUpdate()	Updates the discrete states and work vector state information (i.e. states that are neither continuous nor discrete) saved in work vectors. This routine is invoked by the run-time interface after the major MdlOutputs has been executed.

Function	Description
MdlDerivatives()	Returns the block derivatives. This routine is called in minor steps by the solver during its integration stages. All blocks that have continuous states have an identical number of derivatives. These blocks are required to compute the derivatives so that the solver can integrate the states.
MdlTerminate()	Contains the block shutdown code. The function is called by the run-time interface, as part of the termination of the real-time application.